Chapter 5

Benzothiazole-Triazole Hybrids: Synthesis, Characterization, and Evaluation of Antidiabetic and Anticancer Activities

5.1 Introduction

The design and synthesis of hybrid heterocyclic frameworks is crucial in the quest for new treatments, especially for complex diseases like cancer and diabetes. Benzothiazole and triazole derivatives are distinguished among the extensive variety of heterocycles for their broad spectrum of biological activities. Therapeutically, benzothiazole derivatives exhibit versatility with potent anticancer, antimicrobial, antidiabetic, and antitubercular effects.[262] Meanwhile, triazoles, particularly the 1,2,4- and 1,2,3-triazole isomers, are highly regarded in drug design for their ability to precisely and effectively interact with biological systems.[263]

The focus of this study was the synthesis of innovative hybrid benzothiazole-based compounds, incorporating 1,2,4-triazole, 1,2,3-triazole, Schiff base, and acetamide moieties within a unified molecular structure. The rationale behind this molecular design is grounded in the synergistic potential of these functional groups. Benzothiazole, a well-known pharmacophore, possesses a distinct electronic structure that enables it to interact effectively with biological targets, leading to the suppression of cellular processes.[264] The addition of triazole rings, which are known for their bio-isosteric properties, enhances the flexibility of the molecules, enabling them to function as enzyme inhibitors,[265] DNA intercalators,[266] or receptor modulators,[267] depending on the specific biological environment. The 1,2,4-triazole core has been widely used in designing anticancer drugs because of its beneficial pharmacokinetic properties and its ability to stabilize biologically active conformations through hydrogen bonding networks.[268] Similarly, 1,2,3-triazoles are known for their metal chelating properties, expanding their potential applications in pharmacology.[269]

In addition, Schiff bases have been well-documented as highly effective biological intermediates. They frequently play a critical role in coordinating metals, which is crucial for regulating enzymatic activities and signal transduction pathways.[270,271] On the other

hand, the acetamide component has been included in many biologically active substances because of its lipophilicity, which improves the passage through cell membranes and contributes to positive ADMET (absorption, distribution, metabolism, excretion, and toxicity) characteristics.[272] Thus, combining these moieties into a hybrid scaffold allows for the creation of compounds with optimized biological activity profiles, particularly for diseases such as cancer and diabetes that demand multi-target approaches.

Comprehensive characterization of these hybrid benzothiazole-based compounds was performed using advanced spectroscopic techniques, including ^{1}H NMR, ^{13}C NMR, ^{13}C DEPT NMR, mass spectrometry, and IR spectroscopy, to confirm their structural integrity and purity. The initial evaluation of these compounds involved testing their antidiabetic potential using α-amylase and α-glucosidase inhibition assays. Although the compounds exhibited only moderate inhibitory activity, it was observed that significantly higher concentrations were required in comparison to standard inhibitors. However, this observation has paved the way for a more comprehensive exploration of their pharmacodynamic potential in other biological contexts, with a particular focus on oncology. The hybrid compounds showed highly promising results in their anticancer evaluation against the DTP panel of cancer cell lines, exhibiting potent inhibition against various types of cancer. The inclusion of multiple pharmacophores in the hybrid architecture is essential for the compounds' broad-spectrum cytotoxicity, as it enhances their interference with crucial cellular processes, such as proliferation, survival, and apoptosis. Considering resistance mechanisms that are widespread in contemporary cancer therapies, the capability of these hybrid compounds to target multiple pathways concurrently positions them as compelling contenders for further examination as multi-target anticancer agents.

5.2 Results and discussion

5.2.1 Chemistry

The successful synthesis of the target benzothiazole-based 1,2,4-triazole and 1,2,3-triazole compounds was achieved through a multi-step reaction pathway **(Scheme 1)**. Under reflux conditions, the condensation reaction between 2-aminothiophenol **1** and

diethyl oxalate **2** led to the formation of the intermediate benzothiazole-2-carboxylate **3**. This intermediate underwent reflux with hydrazine hydrate, resulting in the formation of the corresponding hydrazine derivative **4**, which acted as a pivotal constituent for subsequent functionalization. To produce the corresponding dithiocarbazinate salt intermediate **5**, compound **4** was subjected to a reaction with carbon disulfide in the presence of potassium hydroxide in methanol in the next stage. The intermediate **5** underwent cyclization in the presence of hydrazine hydrate under reflux conditions, resulting in the formation of the crucial heterocyclic core 3-thio-1,2,4-triazole benzothiazole **6**.

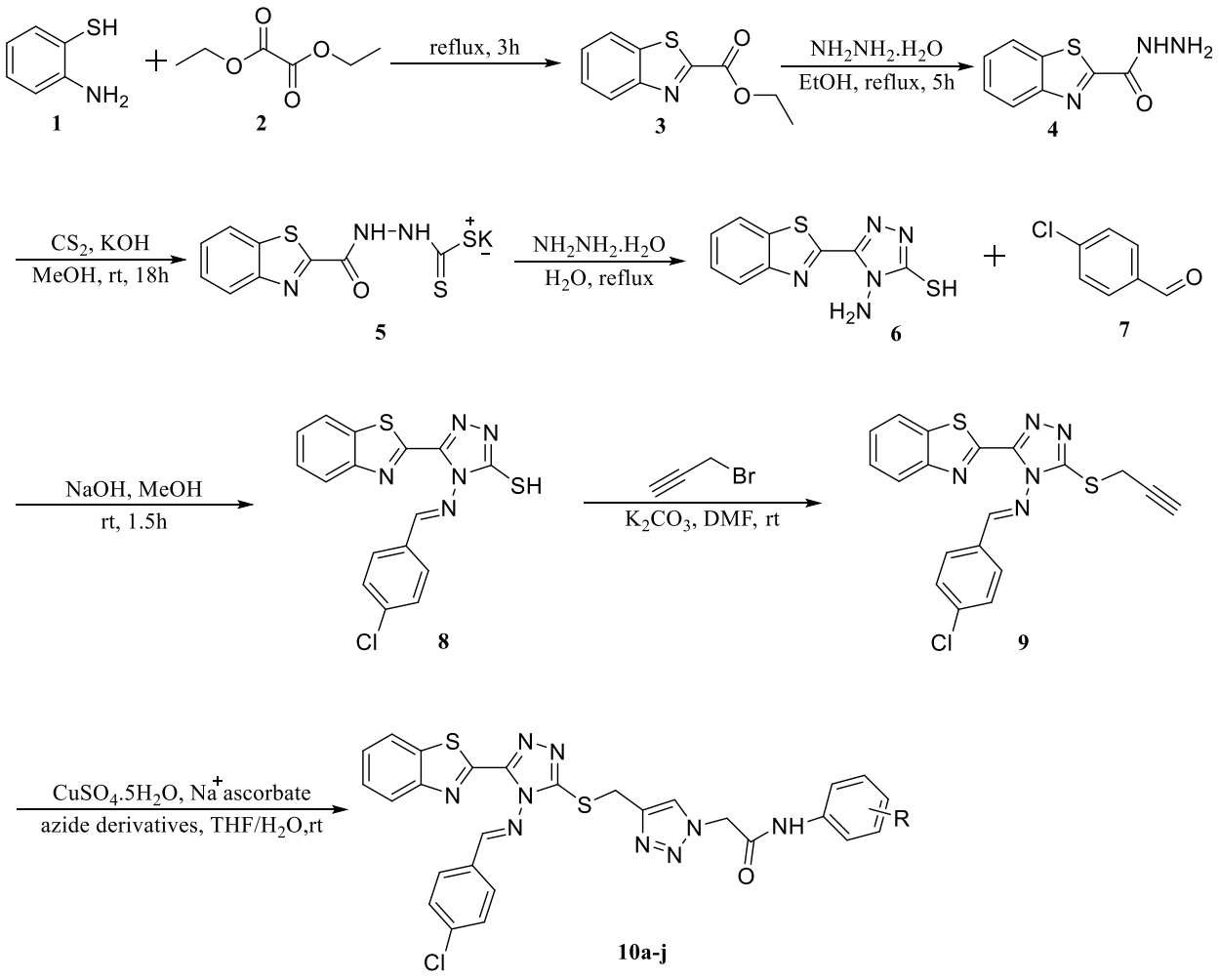

Scheme 1: Synthesis of Benzothiazole-Based 1,2,4-Triazole and 1,2,3-Triazole Derivatives (10a-j) via Multi-Step Reaction Pathway

The preparation of the Schiff base involved the reaction of intermediate **6** with 4-chlorobenzaldehyde, yielding the benzothiazole-triazole Schiff base intermediate **8**. An alkylation reaction was employed to achieve the synthesis of the 1,2,3-triazole hybrid. Deprotonation of the thiol group in compound **8** was achieved by treatment with sodium hydroxide in methanol, followed by nucleophilic substitution with allyl bromide to produce compound **9**. By subjecting the intermediate to a Huisgen cycloaddition, commonly referred to as a "click" reaction, in the presence of $CuSO_4.5H_2O$ and sodium ascorbate in a mixture of THF and water, various azide derivatives were able to form the final benzothiazole derivatives **10a-j** with a 1,2,3-triazole tether. The progress of each synthesis step was tracked using thin-layer chromatography (TLC), and the final compounds were purified through recrystallization with hot ethanol.

The synthesized benzothiazole-based 1,2,4-triazole and 1,2,3-triazole derivatives were comprehensively characterized using ^{1}H NMR, ^{13}C NMR, ^{13}C-DEPT NMR, mass and FT-IR spectroscopy to confirm the molecular structure and integrity of the compounds. The ^{1}H NMR spectrum displayed characteristic signals corresponding to the various proton environments within the molecule. The aromatic protons, originating from both the benzothiazole and phenyl rings, appeared as multiplets in the δ 8.20-6.80 ppm region. The methylene protons (-CH_2-) adjacent to the triazole moiety and amide group were observed as singlets in the range of δ 5.43-4.66 ppm. The amide proton (-NH) was recorded as a broad singlet around δ 10.67-9.65 ppm, indicating the potential for intramolecular hydrogen bonding. The ^{13}C NMR spectrum provided further structural confirmation with the carbonyl carbon (-C=O) of the acetamide group resonating at around δ 169 ppm. The aromatic carbons of the benzothiazole and phenyl rings were observed between δ 164-118 ppm. The methylene carbons (-CH_2-) adjacent to the triazole and amide groups resonated at δ 52-26 ppm. The IR spectrum of the synthesized compound supported these findings, displaying several key absorption bands corresponding to the functional groups present. A strong absorption band at 3200-3400 cm^{-1} was indicative of N-H stretching from the amide group, while the carbonyl (C=O) stretching vibration appeared as a sharp peak around 1650-1700 cm^{-1}.

5.2.2 *In vitro* Antidiabetic evaluation of compound 10a-j

The synthesized benzothiazole-based 1,2,4-triazole and 1,2,3-triazole derivatives were evaluated for their antidiabetic potential by examining their inhibitory activity against the key enzymes α-amylase and α-glucosidase. These enzymes play a crucial role in carbohydrate metabolism, and their inhibition can be a strategic approach to controlling postprandial hyperglycemia in diabetic patients. Acarbose, a known clinical inhibitor of these enzymes, was used as a standard for comparison.

α-Amylase Inhibition Study:

The inhibitory activity of the synthesized compounds against α-amylase was investigated using various concentrations, with acarbose serving as the standard. The results are presented in **Figure 1.**

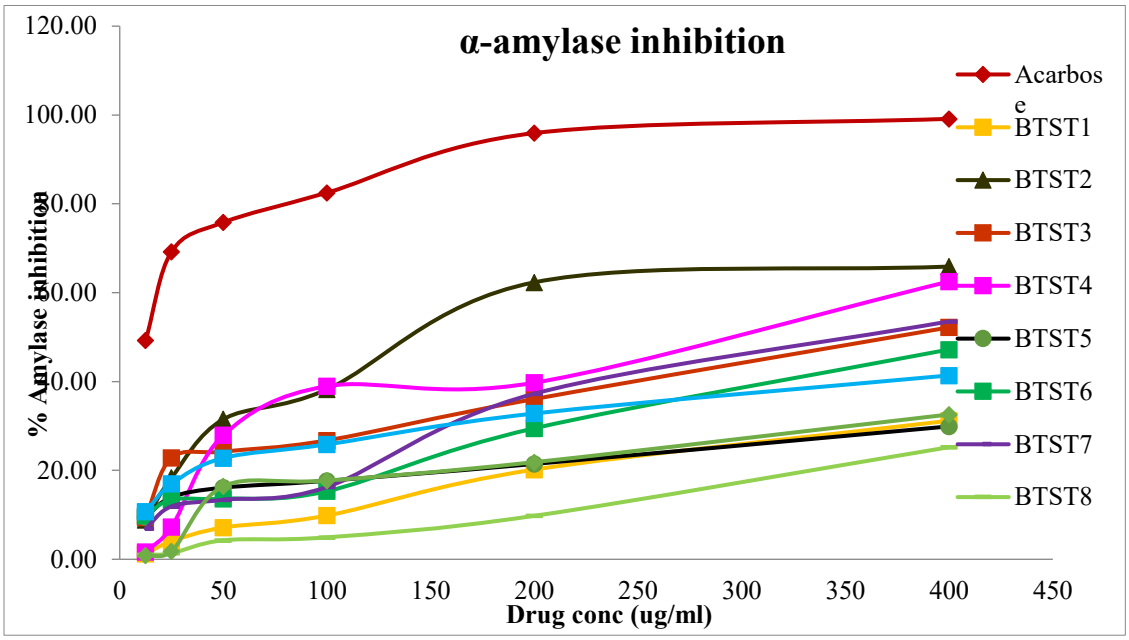

Figure 1: % α-amylase inhibition of synthesized compounds at varying concentrations compared to acarbose

Acarbose exhibited potent inhibition with an IC_{50} value of 15.47 µg/mL. Among the synthesized compounds, **10b** showed the highest α-amylase inhibitory activity with an IC_{50} of 146.72 µg/mL, followed by **10d** (279.26 µg/mL) and **10c** (362.84 µg/mL). The other compounds displayed weaker inhibition, with IC_{50} values exceeding 400 µg/mL, as detailed in **Table 1**. Although **10b** demonstrated a moderate inhibitory effect, it was still

less potent compared to acarbose, suggesting that further structural modifications may be needed to enhance efficacy.

Table 1: IC_{50} values for α-amylase inhibition

α-Amylase enzyme inhibition study-IC_{50} values	
Compounds	IC_{50} (µg/mL)
10a	630.95
10b	146.72
10c	362.84
10d	279.26
10e	827.75
10f	428.92
10g	353.11
10h	817.33
10i	604.47
10j	489.58
Acarbose	15.47

α-Glucosidase Inhibition Study:

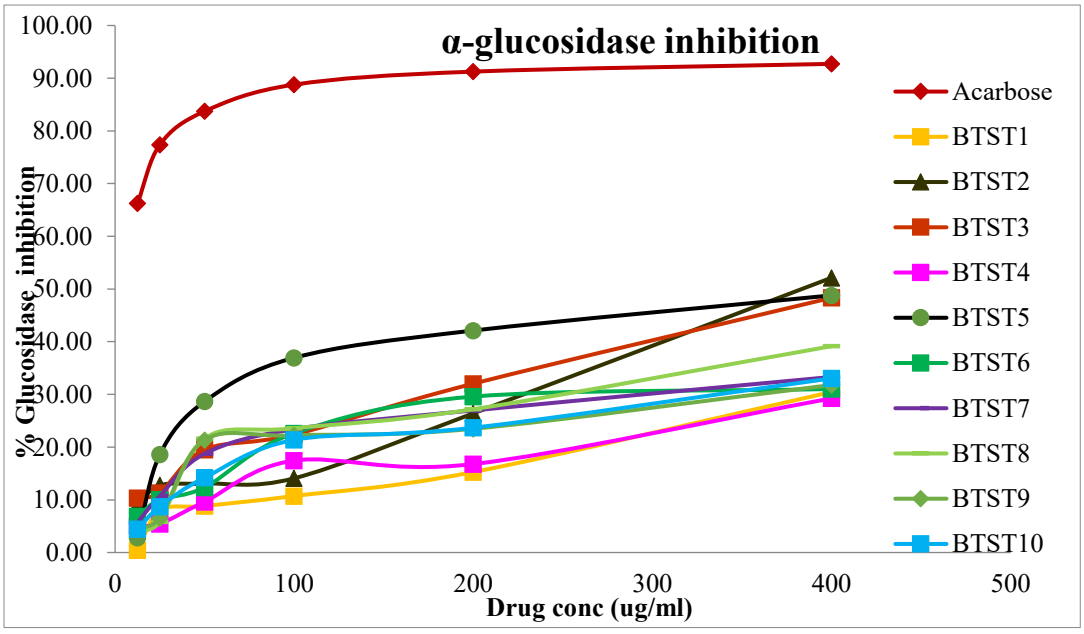

Figure 2: % α-glucosidase inhibition of synthesized compounds at varying concentrations compared to acarbose

In addition to the α-amylase inhibition study, the compounds were also evaluated for their α-glucosidase inhibitory activity. Acarbose once again showed strong inhibition, with an IC_{50} value of 1.3 µg/mL, as shown in **Figure 2**. Among the synthesized compounds, **10b** displayed the highest activity with an IC_{50} value of 396.89 µg/mL, followed by **10c** (404.12 µg/mL) and **10e** (450.31 µg/mL), as summarized in **Table 2**. Despite these results, all of the synthesized compounds required significantly higher concentrations than acarbose to achieve comparable inhibition, indicating that their α-glucosidase inhibitory potential is moderate at best.

Table 2: IC_{50} values for α-glucosidase inhibition

α-Glucosidase enzyme inhibition study-IC_{50} values	
Compound	IC_{50} (µg/mL)
10a	700
10b	396.89
10c	404.12
10d	739.46
10e	450.31
10f	637.63
10g	623.61
10h	502.23
10i	666.73
10j	624.05
Acarbose	1.3

5.2.3 In vitro Anticancer Single Dose assay

The anticancer potential of the synthesized benzothiazole-based triazole derivatives was assessed by subjecting them to a single-dose screening (1 µM) against a total of 60 human cancer cell lines, which were a part of the NCI Developmental Therapeutics Program. In this panel, there is an extensive coverage of cancer types including leukemia, non-small cell lung cancer (NSCLC), colon cancer, CNS cancer, melanoma, ovarian cancer, renal cancer, prostate cancer, and breast cancer. The results from Figures 3-12

demonstrate that certain compounds displayed notable cytotoxic effects on various cancer cell lines, suggesting their potential as effective anticancer agents.

It was observed through the single-dose screening that certain compounds displayed notable effectiveness in inhibiting the proliferation of cancer cells. The colon cancer panel demonstrated remarkable inhibition by compound **10g**, achieving growth inhibition values of -95.41% and -96.41% in SW-620 and HCT-116 cell lines, respectively. Moreover, this compound demonstrated potent activity against ovarian cancer cell lines SK-OV-3 and OVCAR-8, inhibiting them by over 98%. The results of these findings indicate that **10g** exhibits a wide range of effectiveness, with notable impact on colon and ovarian cancers in particular. In a similar manner, compound **10c** demonstrated strong inhibitory effects against the melanoma panel. Notably, cell lines such as LOX IMVI and SK-MEL-2 exhibited significant sensitivity to the compound, resulting in growth inhibitions of -92.23% and -83.70%, respectively. The compound's efficacy against breast cancer cell lines, especially MCF7, was highlighted by a significant growth inhibition of -72.90%. The fact that **10c** shows a robust anticancer profile in various types of cancer underscores its promise for further exploration.

The efficacy of Compound **10d** in multiple cancer types was noteworthy, particularly its exceptional activity demonstrated in both CNS and ovarian cancer panels. The compound proved to be highly effective in suppressing the growth of cancer cells, particularly in the CNS cancer cell line SF-539, where it demonstrated an outstanding inhibition rate of -95.91%. Moreover, it exhibited a comparable level of potency in the ovarian cancer cell line SK-OV-3, resulting in a notable reduction of -94.99%. The findings from this research strongly suggest that **10d** holds significant promise in treating these aggressive cancer types. Therefore, it is crucial to pursue additional research to fully explore and understand its therapeutic potential.

Additionally, compound **10e** exhibited strong inhibition against CNS and breast cancer cell lines. SF-539 and SNB-75 CNS cell lines displayed a remarkable reduction in growth by -97.24% and -83.65% respectively. Similarly, the breast cancer cell line MCF7 also showed significant sensitivity to **10e** with a decrease in growth by 74.10%. The compound's ability to effectively target a wide range of cancer types suggests that it could

be a promising candidate for developing anticancer treatments. Apart from these results, compound **10i** displayed remarkable efficacy against melanoma and breast cancer, specifically demonstrating high responsiveness towards LOX IMVI (-99.56%) and MCF7 (-95.48%). The significant ability of **10i** to inhibit these specific cancer cell lines emphasizes its potential as a targeted treatment option for melanoma and breast cancer.

The synthesized triazole derivatives based on benzothiazole demonstrated a diverse array of anticancer activities, with multiple compounds showing significant cytotoxicity against various cancer types. Strong candidates for further investigation, specifically in melanoma, ovarian, and breast cancers, include compounds such as **10g**, **10c**, **10d**, **10e**, and **10i**. The notable suppression of growth observed in these compounds in various types of cancer underscores their potential as candidates for therapeutic development. The growth inhibition percentages across the 60 cancer cell lines for each compound are visualized in Figures 3-12 as part of the anticancer screening results. These data offer a complete perspective on the compounds' ability to halt cell growth and kill cells, further bolstering their potential in the development of anticancer drugs.

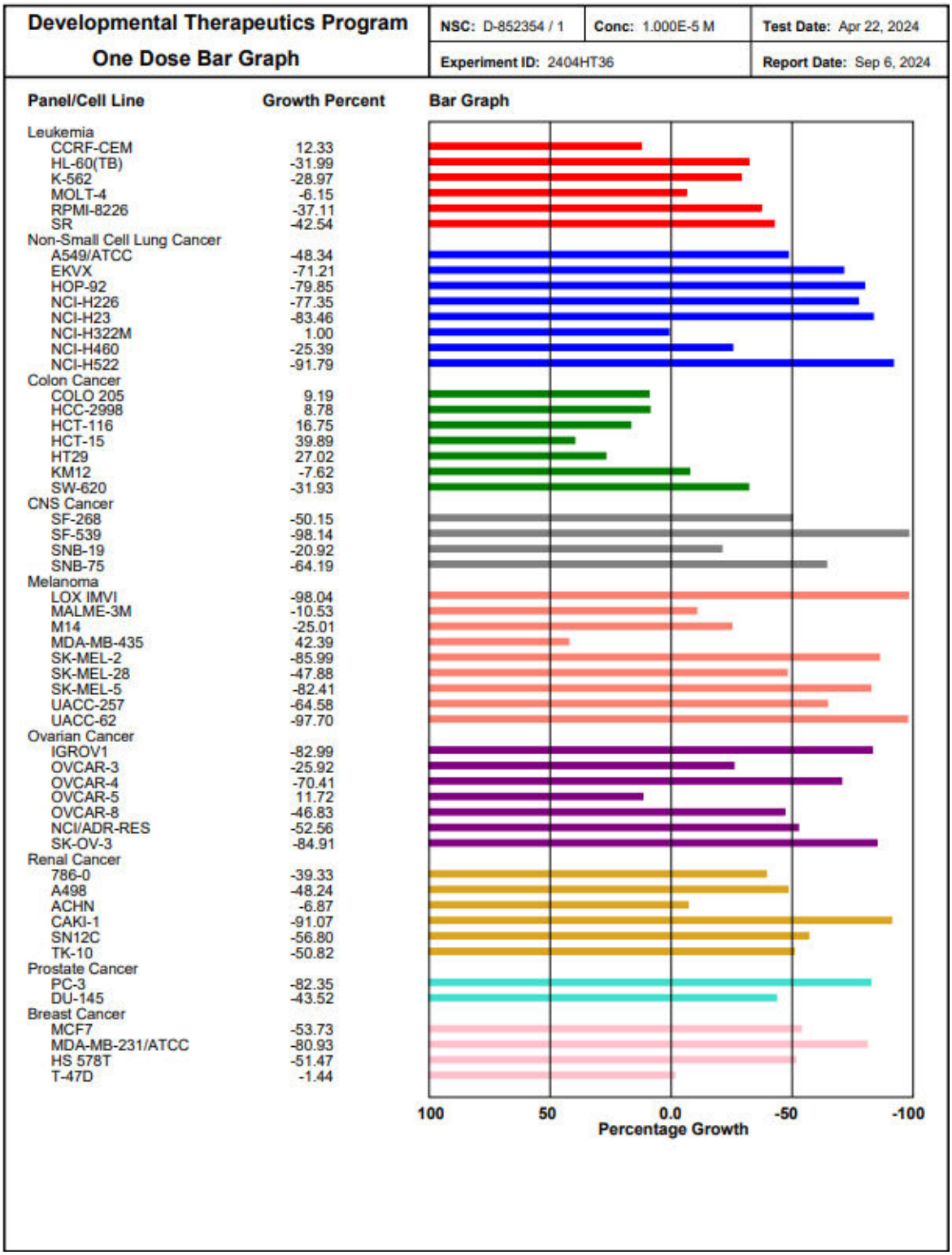

Figure 3: Single dose data for compound 10a

Developmental Therapeutics Program

One Dose Bar Graph

NSC: D-852355 / 1	Conc: 1.000E-5 M	Test Date: Apr 22, 2024
Experiment ID: 2404HT36		Report Date: Sep 6, 2024

Panel/Cell Line	Growth Percent
Leukemia	
CCRF-CEM	0.08
HL-60(TB)	-51.72
K-562	7.37
MOLT-4	11.76
RPMI-8226	-4.59
SR	7.94
Non-Small Cell Lung Cancer	
A549/ATCC	57.38
EKVX	-11.77
HOP-92	-5.90
NCI-H226	-3.78
NCI-H23	24.33
NCI-H322M	62.17
NCI-H460	-1.19
NCI-H522	-31.23
Colon Cancer	
COLO 205	90.13
HCC-2998	52.11
HCT-116	62.34
HCT-15	51.05
HT29	38.25
KM12	16.18
SW-620	-18.58
CNS Cancer	
SF-268	-86.35
SF-539	-15.76
SNB-19	37.47
SNB-75	-14.71
Melanoma	
LOX IMVI	7.29
MALME-3M	-17.30
M14	2.33
MDA-MB-435	13.15
SK-MEL-2	-43.34
SK-MEL-28	5.11
SK-MEL-5	15.37
UACC-257	36.85
UACC-62	-67.69
Ovarian Cancer	
IGROV1	6.83
OVCAR-3	-3.62
OVCAR-4	18.85
OVCAR-5	70.52
OVCAR-8	70.15
NCI/ADR-RES	41.93
SK-OV-3	58.44
Renal Cancer	
786-0	84.02
A498	28.48
ACHN	66.67
CAKI-1	-4.93
SN12C	-8.53
TK-10	-42.87
Prostate Cancer	
PC-3	31.78
DU-145	-9.85
Breast Cancer	
MCF7	-8.14
MDA-MB-231/ATCC	15.40
HS 578T	-18.12
T-47D	60.15

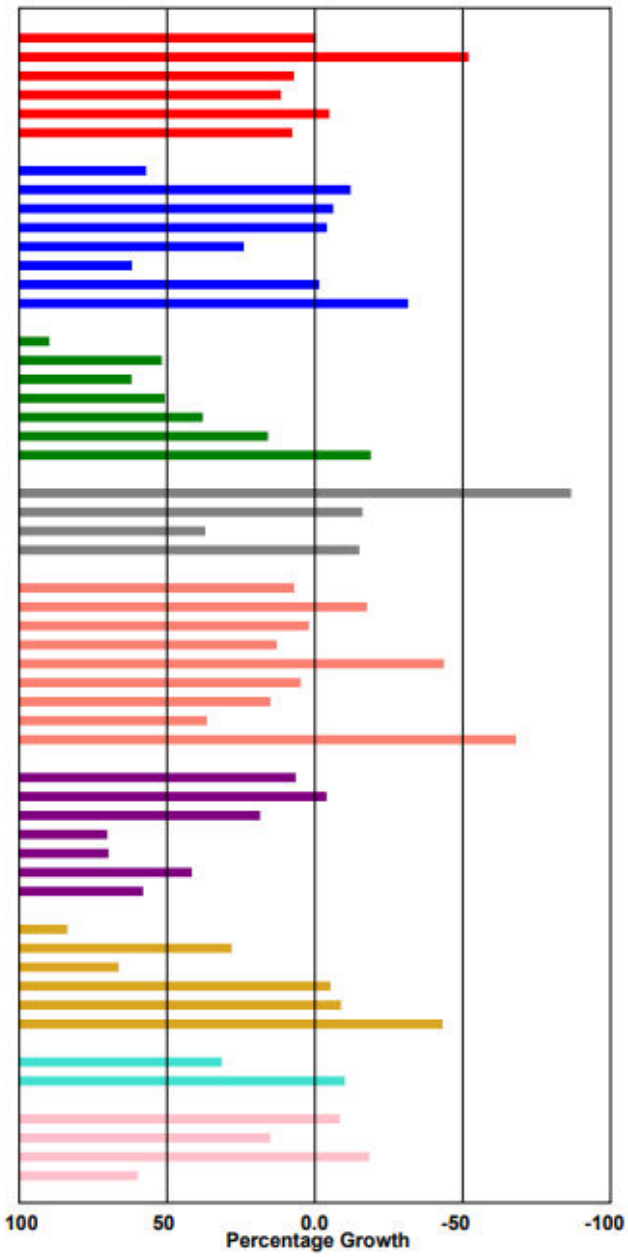

Figure 4: single dose data for compound 10b

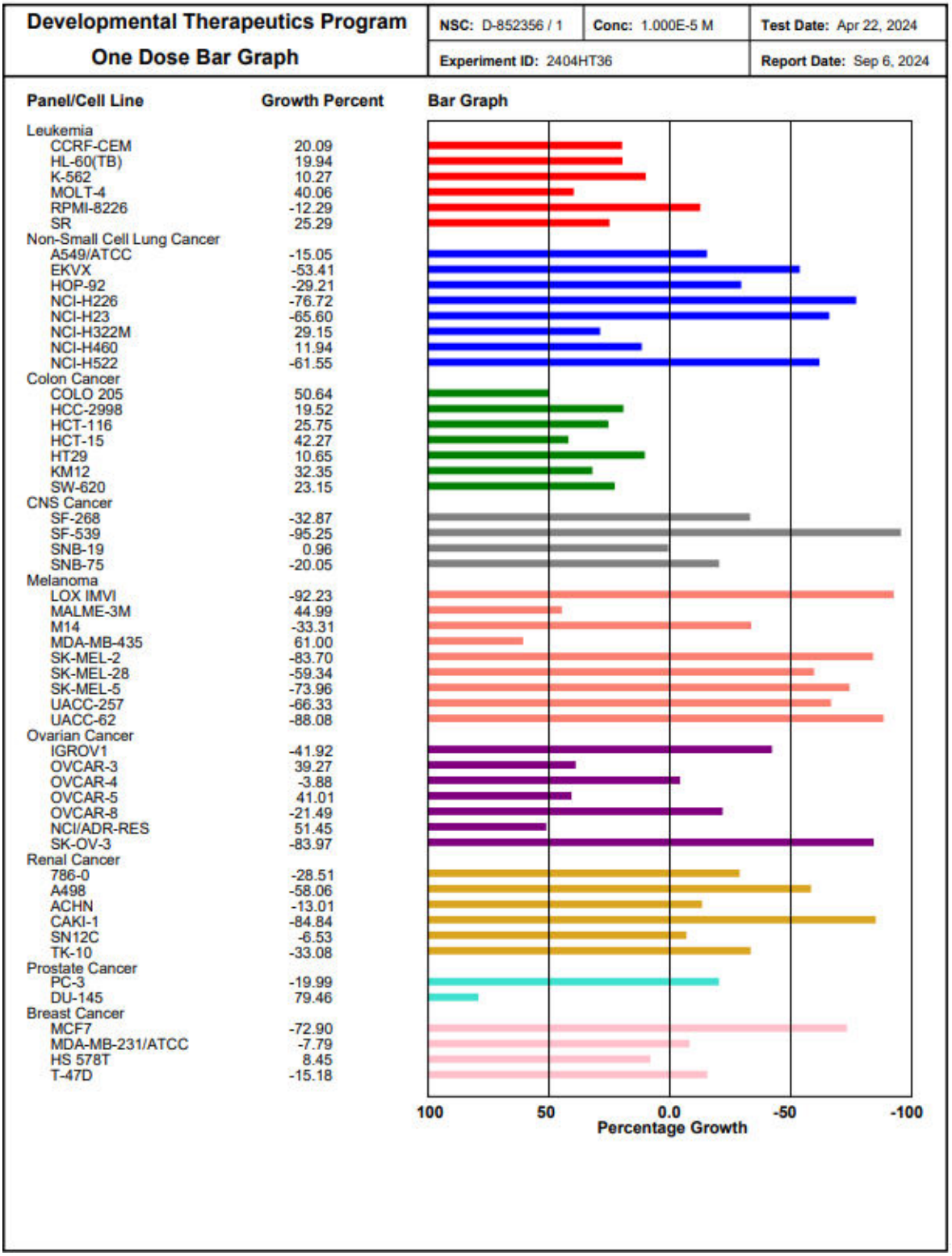

Figure 5: Single dose data for compound 10c

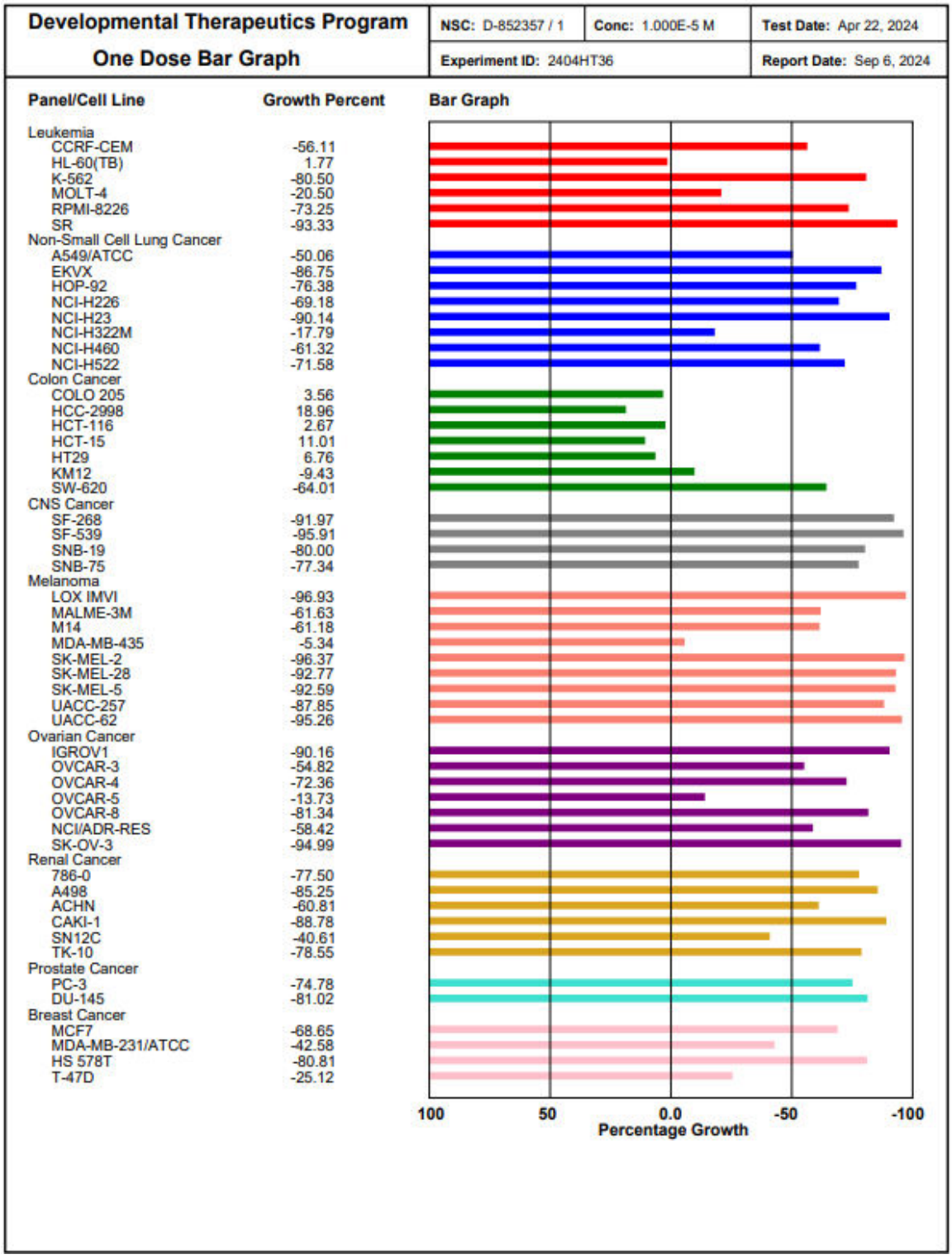

Figure 6: Single dose data for compound 10d

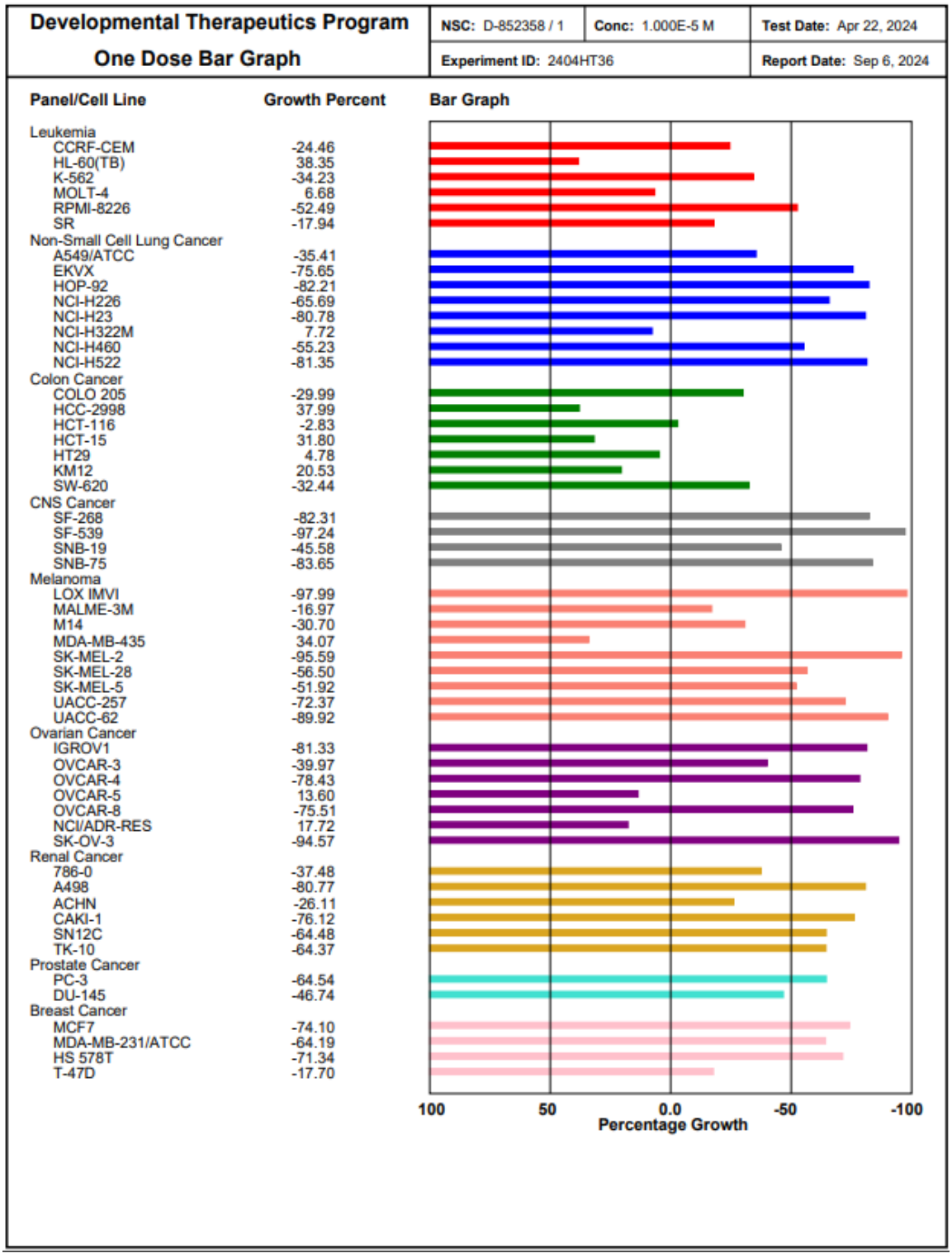

Developmental Therapeutics Program

One Dose Bar Graph

NSC: D-852358 / 1	Conc: 1.000E-5 M	Test Date: Apr 22, 2024
Experiment ID: 2404HT36		Report Date: Sep 6, 2024

Panel/Cell Line	Growth Percent
Leukemia	
CCRF-CEM	-24.46
HL-60(TB)	38.35
K-562	-34.23
MOLT-4	6.68
RPMI-8226	-52.49
SR	-17.94
Non-Small Cell Lung Cancer	
A549/ATCC	-35.41
EKVX	-75.65
HOP-92	-82.21
NCI-H226	-65.69
NCI-H23	-80.78
NCI-H322M	7.72
NCI-H460	-55.23
NCI-H522	-81.35
Colon Cancer	
COLO 205	-29.99
HCC-2998	37.99
HCT-116	-2.83
HCT-15	31.80
HT29	4.78
KM12	20.53
SW-620	-32.44
CNS Cancer	
SF-268	-82.31
SF-539	-97.24
SNB-19	-45.58
SNB-75	-83.65
Melanoma	
LOX IMVI	-97.99
MALME-3M	-16.97
M14	-30.70
MDA-MB-435	34.07
SK-MEL-2	-95.59
SK-MEL-28	-56.50
SK-MEL-5	-51.92
UACC-257	-72.37
UACC-62	-89.92
Ovarian Cancer	
IGROV1	-81.33
OVCAR-3	-39.97
OVCAR-4	-78.43
OVCAR-5	13.60
OVCAR-8	-75.51
NCI/ADR-RES	17.72
SK-OV-3	-94.57
Renal Cancer	
786-0	-37.48
A498	-80.77
ACHN	-26.11
CAKI-1	-76.12
SN12C	-64.48
TK-10	-64.37
Prostate Cancer	
PC-3	-64.54
DU-145	-46.74
Breast Cancer	
MCF7	-74.10
MDA-MB-231/ATCC	-64.19
HS 578T	-71.34
T-47D	-17.70

Bar Graph

100 50 0.0 -50 -100

Percentage Growth

Figure 7: Single dose data for compound 10e

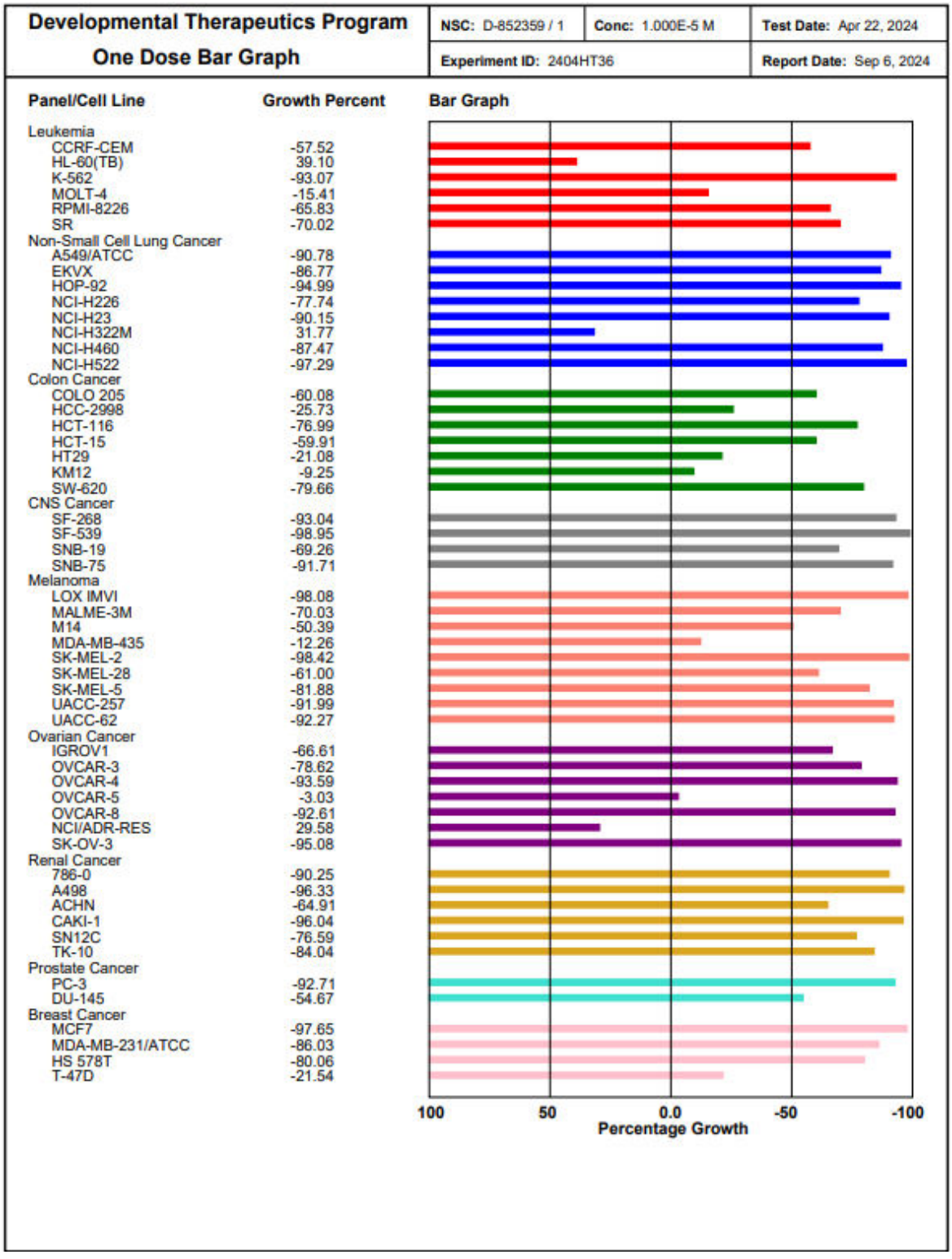

Figure 8: single dose data for compound 10f

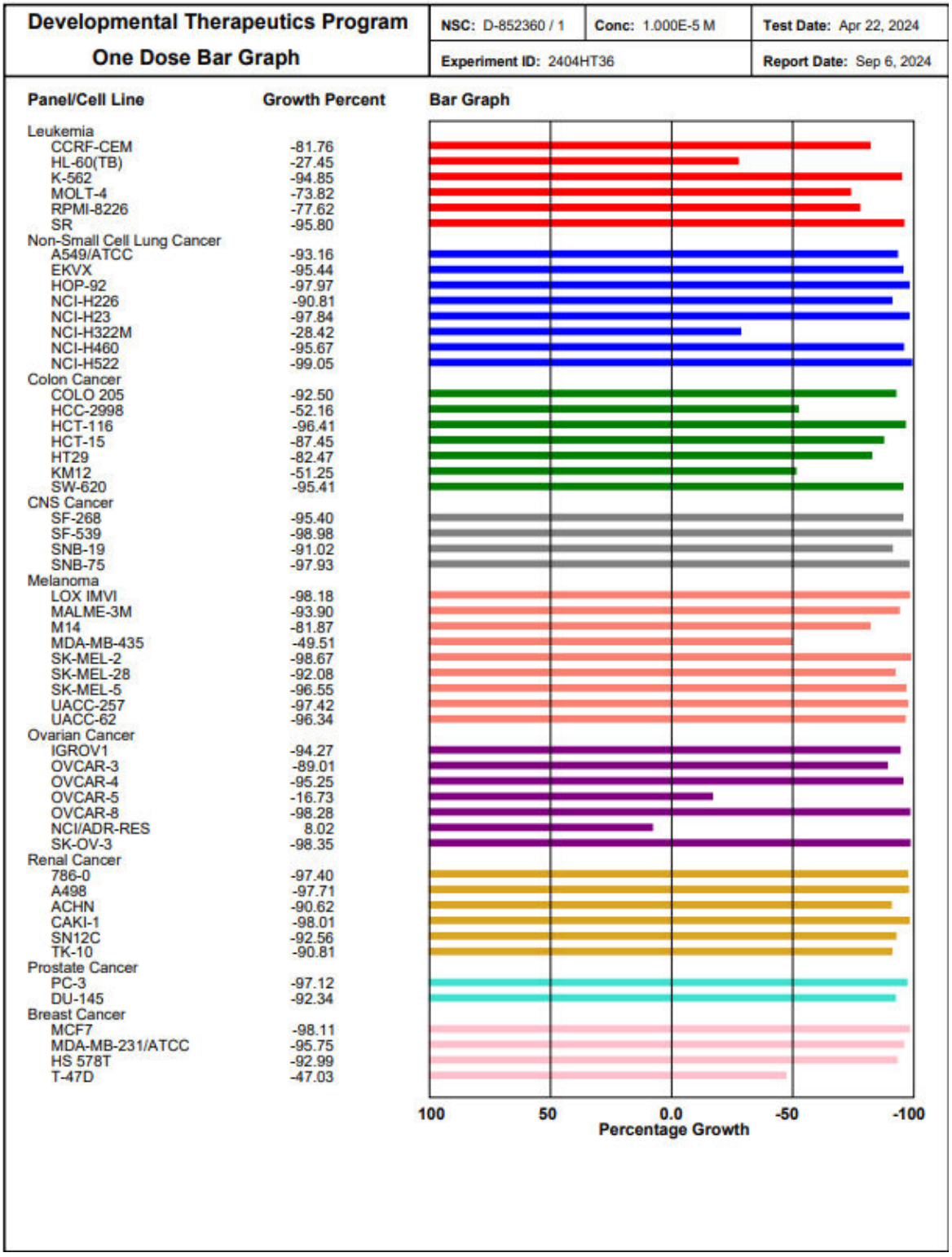

Developmental Therapeutics Program

One Dose Bar Graph

NSC: D-852360 / 1	Conc: 1.000E-5 M	Test Date: Apr 22, 2024
Experiment ID: 2404HT36		Report Date: Sep 6, 2024

Panel/Cell Line	Growth Percent
Leukemia	
CCRF-CEM	-81.76
HL-60(TB)	-27.45
K-562	-94.85
MOLT-4	-73.82
RPMI-8226	-77.62
SR	-95.80
Non-Small Cell Lung Cancer	
A549/ATCC	-93.16
EKVX	-95.44
HOP-92	-97.97
NCI-H226	-90.81
NCI-H23	-97.84
NCI-H322M	-28.42
NCI-H460	-95.67
NCI-H522	-99.05
Colon Cancer	
COLO 205	-92.50
HCC-2998	-52.16
HCT-116	-96.41
HCT-15	-87.45
HT29	-82.47
KM12	-51.25
SW-620	-95.41
CNS Cancer	
SF-268	-95.40
SF-539	-98.98
SNB-19	-91.02
SNB-75	-97.93
Melanoma	
LOX IMVI	-98.18
MALME-3M	-93.90
M14	-81.87
MDA-MB-435	-49.51
SK-MEL-2	-98.67
SK-MEL-28	-92.08
SK-MEL-5	-96.55
UACC-257	-97.42
UACC-62	-96.34
Ovarian Cancer	
IGROV1	-94.27
OVCAR-3	-89.01
OVCAR-4	-95.25
OVCAR-5	-16.73
OVCAR-8	-98.28
NCI/ADR-RES	8.02
SK-OV-3	-98.35
Renal Cancer	
786-0	-97.40
A498	-97.71
ACHN	-90.62
CAKI-1	-98.01
SN12C	-92.56
TK-10	-90.81
Prostate Cancer	
PC-3	-97.12
DU-145	-92.34
Breast Cancer	
MCF7	-98.11
MDA-MB-231/ATCC	-95.75
HS 578T	-92.99
T-47D	-47.03

Bar Graph

100 50 0.0 -50 -100

Percentage Growth

Figure 9: Single dose data for compound 10g

Developmental Therapeutics Program

One Dose Bar Graph

NSC: D-852361 / 1	Conc: 1.000E-5 M	Test Date: Apr 22, 2024
Experiment ID: 2404HT36		Report Date: Sep 6, 2024

Panel/Cell Line	Growth Percent
Leukemia	
CCRF-CEM	49.73
HL-60(TB)	85.12
K-562	46.41
MOLT-4	44.59
RPMI-8226	38.33
SR	10.78
Non-Small Cell Lung Cancer	
A549/ATCC	52.24
EKVX	-31.72
HOP-92	-0.41
NCI-H226	-11.63
NCI-H23	32.30
NCI-H322M	69.27
NCI-H460	31.09
NCI-H522	-71.86
Colon Cancer	
COLO 205	86.61
HCC-2998	57.07
HCT-116	36.53
HCT-15	65.94
HT29	75.72
KM12	50.33
SW-620	59.92
CNS Cancer	
SF-268	-5.97
SF-539	-54.65
SNB-19	48.99
SNB-75	-19.86
Melanoma	
LOX IMVI	-90.14
MALME-3M	16.30
M14	20.76
MDA-MB-435	91.83
SK-MEL-2	-56.76
SK-MEL-28	12.49
SK-MEL-5	-4.90
UACC-257	-14.27
UACC-62	0.03
Ovarian Cancer	
IGROV1	-38.41
OVCAR-3	28.83
OVCAR-4	27.61
OVCAR-5	62.62
OVCAR-8	18.15
NCI/ADR-RES	60.70
SK-OV-3	-7.82
Renal Cancer	
786-0	46.33
A498	17.21
ACHN	19.72
CAKI-1	-86.66
SN12C	48.14
TK-10	5.89
Prostate Cancer	
PC-3	33.47
DU-145	50.31
Breast Cancer	
MCF7	0.16
MDA-MB-231/ATCC	11.24
HS 578T	-7.55
T-47D	-1.96

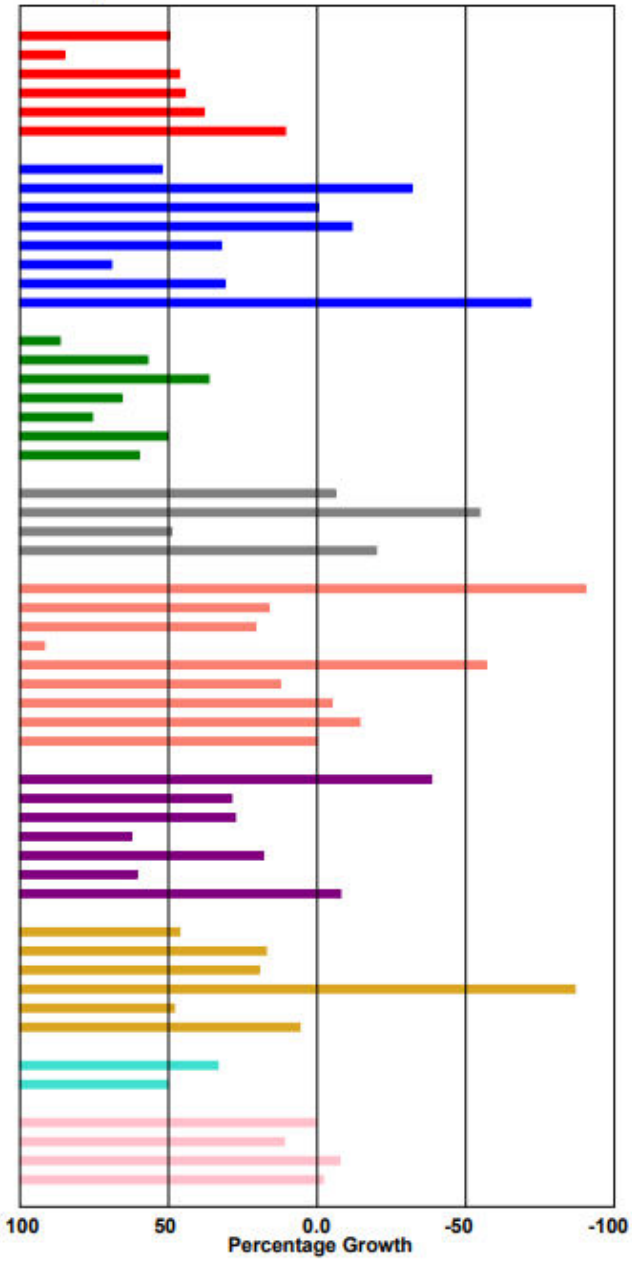

Figure 10: Single dose data for compound 10h

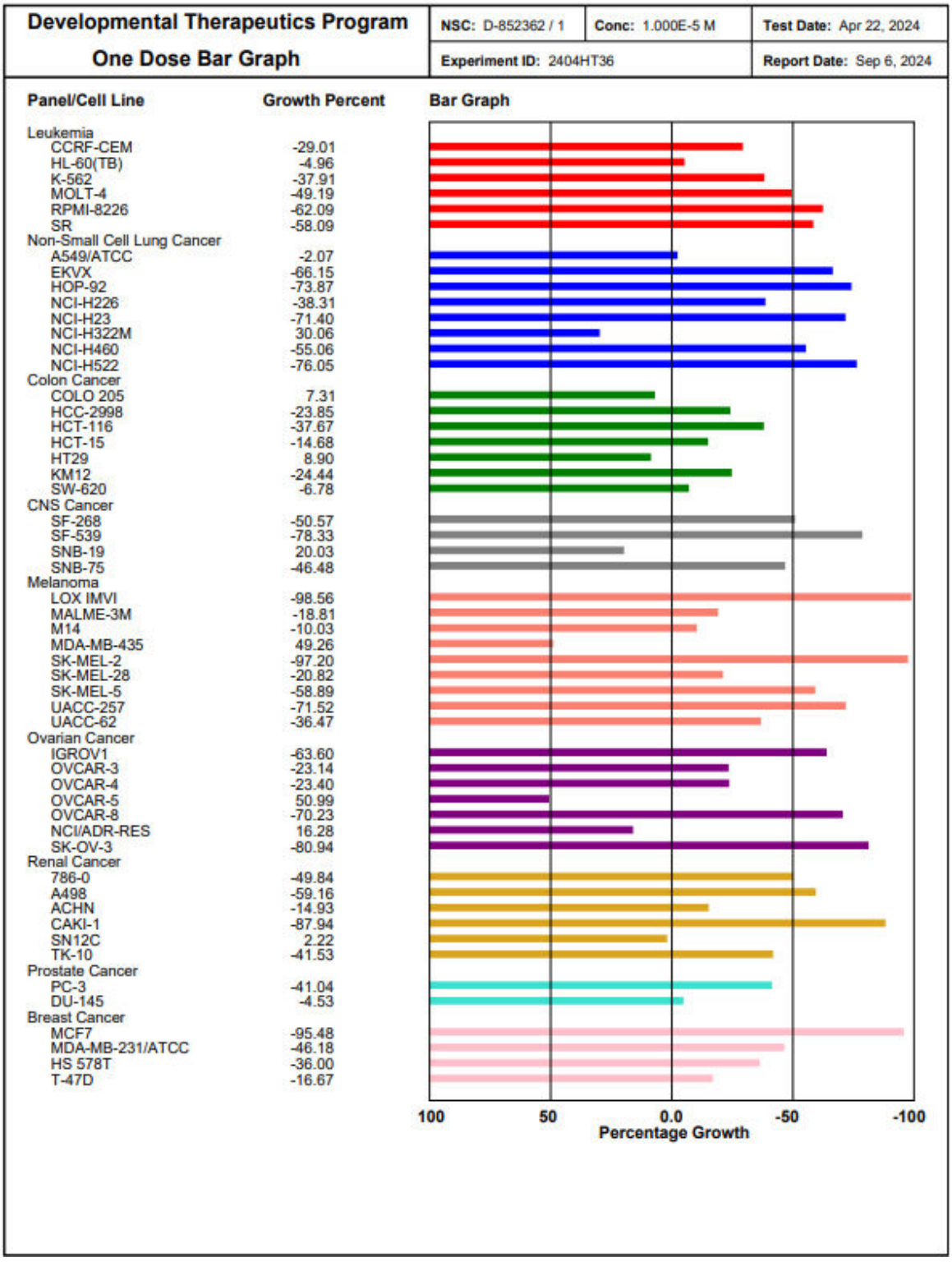

Figure 11: Single dose data for compound 10i

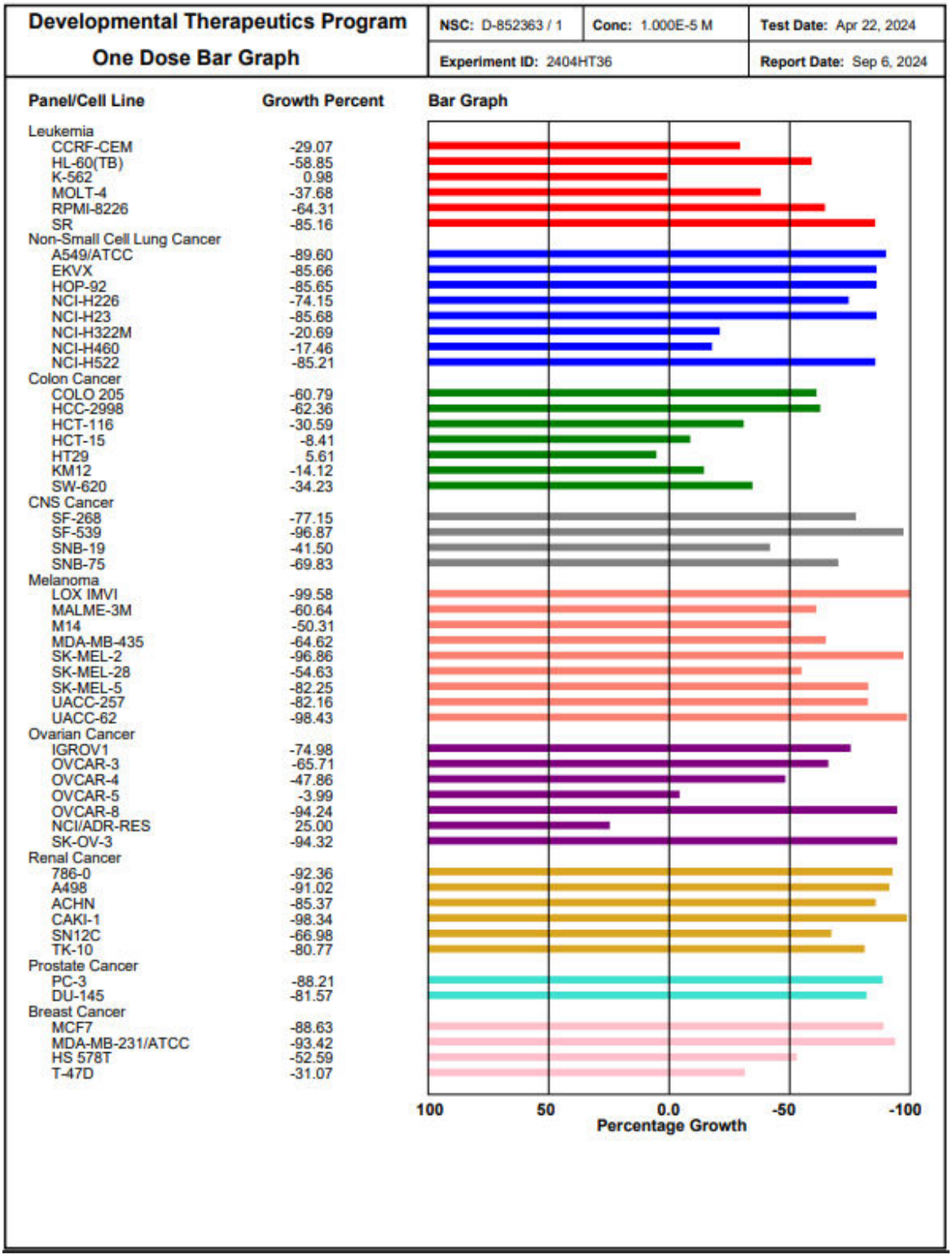

Figure 12: Single dose data for compound 10j

5.3 Material and method

5.3.1 Chemistry

All the chemicals and reagents employed were of analytical grade, ensuring no additional purification was necessary. The NMR spectra, including ^{1}H NMR and ^{13}C NMR, were obtained using an AvanceNeo Ascend spectrometer operating at a frequency of 400 MHz for proton NMR and 101 MHz for carbon NMR. The measurements were conducted in DMSO-d_6, and the chemical shifts were reported in δ ppm relative to TMS. The acquisition of mass spectra was conducted by utilizing a direct inlet method on a Waters ACQUITY QDa spectrometer. Using the KBr pellet method, the FT-IR spectra were recorded on a Shimadzu FTIR-8400 spectrometer, offering precise and reliable results. The electrothermal device from Tempo Instruments was used to measure the melting points, which were uncorrected, using open capillaries. The execution of thin-layer chromatography (TLC) involved the utilization of Silica Gel 60 F254 TLC Aluminum Sheets (Merck KGaA, Darmstadt, Germany), with the visualization of spots occurring under UV light at wavelengths of 254 nm and 365 nm.

- **General procedure for the synthesis of benzothiazole-2-carboxylate (3)**

  A reflux reaction was performed on a mixture comprising 20 mmol of diethyl oxalate **1** and 10 mmol of 2-aminothiophenol **2** for 5 hours. TLC was employed to confirm the completion of the reaction, with a solvent system consisting of ethyl acetate and n-hexane in a 2:1 ratio. The mixture was cooled and subsequently agitated with 50 mL of methanol for a period of 30 minutes. Following that, it was combined with a solution containing 20 mL of HCl and 80 mL of water, and vigorously mixed. The white solid that formed was isolated using vacuum filtration, dried, and then recrystallized from methanol. This process resulted in a 94% yield of benzothiazole-2-carboxylate **3** as a white solid.

- **Standard protocol for synthesis of benzothiazole-2-carbohydrazide (4)**

  A solution of 10 mmol of benzothiazole-2-carboxylate **3** was prepared by dissolving it in 50 mL of absolute ethanol. The solution underwent drop-wise addition of hydrazine hydrate (99%), which was subsequently refluxed for 6 hours. TLC was employed to monitor the advancement of the reaction, employing a solvent blend

of ethyl acetate and n-hexane in a 2:1 ratio. After the reaction was finished, the mixture was cooled to room temperature, underwent vacuum filtration, rinsed with water, and left to dry overnight. The procedure led to a 86% yield of yellow benzothiazole-2-carbohydrazide **4**.

- **Synthesis of potassium 2-(benzo[d]thiazole-2-carbonyl) hydrazine-1-carbodithioate salt (5)**

  A methanolic solution of potassium hydroxide (15 mmol) was used to dissolve Benzothiazole-2-carbohydrazide **4** (10 mmol), followed by stirring at room temperature. Sequentially, carbon disulfide (15 mmol) was added drop by drop to the mixture, which was subsequently stirred continuously for 18 hours. The completion of the reaction was confirmed through TLC analysis. Consequently, the reaction mixture was subjected to vacuum filtration, and the solid that was obtained underwent multiple washes with diethyl ether. The product was carefully dried in an oven maintained at a temperature of 80°C for 3 hours. The yellow salt potassium 2-(benzo[d]thiazole-2-carbonyl) hydrazine-1-carbodithioate **5** was successfully obtained with a yield of 92%. With no additional purification, this salt was employed in the following reaction.

- **General method for Synthesis of 4-amino-5-(benzo[d]thiazol-2-yl)-4H-1,2,4-triazole-3-thiol moiety (6)**

  Initially, a solution was prepared by dissolving 10 mmol of potassium dithiocarbazinate salt **5** in water, followed by the gradual addition of hydrazine hydrate (99%, 20 mmol) drop by drop. The solution underwent reflux conditions and was heated to a temperature of 90°C. During the course of the reaction, the liberation of hydrogen sulfide gas occurred, and its presence was verified by the discernible alteration in the color of a lead acetate-soaked filter paper, transitioning from a white hue to a black hue. After the completion of the hydrogen sulfide gas evolution, the reaction mixture was subsequently cooled to room temperature and subjected to a workup utilizing a 20% hydrochloric acid solution in water. The resulting slight yellow precipitate was obtained via vacuum filtration, subsequently purified with hot ethanol, and ultimately dried in an oven at 100°C. As a result of this process, a white solid in the form of pure 4-amino-5-(benzo[d]thiazol-2-yl)-

4H-1,2,4-triazole-3-thiol **6** was obtained. Yield 90%; White solid; mp: 221-223 ℃; ^{1}H NMR (400 MHz, DMSO-d_6): δ 14.38 (s, 1H, SH), 8.29–8.22 (d, 1H, Ar–H), 8.21–8.14 (d, 1H, Ar–H), 7.61 (dddd, J = 22.4, 8.4, 7.2, 1.3 Hz, 2H, Ar–H), 6.19 (s, 2H, NH_2); ^{13}C NMR (101 MHz, DMSO-d_6) δ 167.36 (C–SH), 152.55 (C–C), 144.94 (C–C),152.49, 135.15, 127.52, 127.14, 124.05, 122.91 (Ar–C); (ESI-MS) m/z 249.90 $(M+H)^+$.

- **Standard procedure for Synthesis of (E)-5-(benzo[d]thiazol-2-yl)-4-(benzylideneamino)-4H-1,2,4-triazole-3-thiol (8)**

  A solution was prepared by dissolving 10 mmol of the compound 4-amino-5-(benzo[d]thiazol-2-yl)-4H-1,2,4-triazole-3-thiol 6 in 20 mL of methanol, followed by sonication for 5 minutes. The suspension was treated with 10 mmol of NaOH and agitated at room temperature until complete dissolution of all reactants. Following a period of 30 minutes, the compound 4-chlorobenzaldehyde **7** (11 mmol), was introduced to the solution and subsequently mixed at ambient temperature. The precipitates that were produced as a result of the reaction were carefully filtered using a vacuum filtration system. Following the filtration process, the precipitates were thoroughly washed with water and then set aside to dry overnight at room temperature. Following that, a wash was performed using hot ethanol in order to obtain a pure form of intermediate 8. Yield 96%; Light yellow solid; mp 173-175 ℃; IR (KBr): *v* 2901 (C-H alkane stre.), 1643 (C=N stre.), 1280 (C-N stre.); ^{1}H NMR (400 MHz, DMSO- d_6): δ 14.70 (s, 1H, SH), 9.87 (s, 1H, HC=N), 8.26 (d, *J* = 7.8 Hz, 1H, Ar-H), 8.11 (d, *J* = 7.8 Hz, 1H, Ar-H), 8.06–8.04 (m, 2H, Ar-H), 7.71 (dd, *J* = 8.5, 5.9 Hz, 1H. Ar-H), 7.69–7.55 (m, 4H, Ar-H) ppm; ^{13}C NMR (101 MHz, DMSO- d_6) δ 167.45 (C-SH), 153.40 (C-C), 152.67, 151.99 (HC=N), 135.61, 135.51, 132.30, 129.86, 129.64, 127.28, 124.25, 123.40, 123.04 (Ar-C) ppm; MS *m/z* (M+1): 338.1. Aanl. Calcd. for $C_{16}H_{11}N_5S_2$: C, 56.95; H, 3.29; N, 20.76. Found C, 56.90; H, 3.25; N, 20.73%.
- **Standard procedure for Synthesis of (E)-N-(3-(benzo[d]thiazol-2-yl)-5-(prop-2-yn-1-ylthio)-4H-1,2,4-triazol-4-yl)-1-(4-chlorophenyl)methanimine (9)**

  Compound **8** was dissolved in DMF, followed by the addition of K_2CO_3 (15 mmol). The mixture was stirred for 15 minutes, after which propargyl bromide (15 mmol)

was added. The reaction was stirred for 12 hours. Upon completion, the reaction mixture was poured into water, washed thoroughly with excess water, vacuum filtered, and dried at room temperature. The resulting product, compound **9**, was used without further purification.

- **General procedure for Synthesis of (E)-2-(4-(((5-(benzo[d]thiazol-2-yl)-4-((4-chlorobenzylidene)amino)-4H-1,2,4-triazol-3-yl)thio)methyl)-1H-1,2,3-triazol-1-yl)-N-phenylacetamide derivatives (10a-j)**

  The obtained product **9** was further subjected to a CuAAC click reaction. Compound **9** was dissolved in a THF/water mixture (9:2), and $CuSO_4.5H_2O$ (4 mol%) was added, followed by the addition of sodium ascorbate (2 mol%). The mixture was stirred for 15 minutes, after which the prepared azide derivatives (12 mmol) were introduced, and the reaction was allowed to stir at room temperature for 6 hours. Upon completion, the reaction mixture was poured into an aqueous NH_4Cl solution, washed with excess water, and purified by washing with hot ethanol to obtain the pure derivatives **10a-j**.

- **(E)-2-(4-(((5-(benzo[d]thiazol-2-yl)-4-((4-chlorobenzylidene)amino)-4H-1,2,4-triazol-3-yl)thio)methyl)-1H-1,2,3-triazol-1-yl)-N-(2,4-dimethylphenyl)acetamide (10a)**

  Yield 93%; Reddish orange; mp 195-197 °C; FT-IR (KBr, ν, cm^{-1}): 3255.95 (NH Stretch), 1666.55 (amide Stretch); ^1H NMR (400 MHz, DMSO) δ 9.69 (s, 1H, NH), 9.23 (s, 1H, HC=N), 8.21 (dd, *J* = 6.2, 3.2 Hz, 1H, Ar-H), 8.13 (s, 1H, CH, Ar-H), 7.98–7.96 (d, *J* = 8.1 Hz, 2H, Ar-H), 7.85 (m, 1H, Ar-H), 7.70–7.68 (d, *J* = 8.1 Hz, 2H, Ar-H), 7.55–7.54 (m, 2H, Ar-H), 7.24–7.22 (d, *J* = 8.0 Hz, 1H, Ar-H), 6.99 (s, 1H, Ar-H), 6.89–6.87 (d, *J* = 8.1 Hz, 1H, Ar-H), 5.34 (s, 2H, CH_2), 4.67 (s, 2H, CH_2), 2.21 (s, 3H, CH_3), 2.15 (s, 3H, CH_3); ^{13}C NMR (101 MHz, DMSO) δ 169.98 (C=O), 164.69 (C-S), 154.65 (C=N), 152.96, 145.82, 138.70, 135.12, 134.60, 133.27, 131.92, 131.36, 130.69, 130.07, 127.48, 127.20, 126.97, 126.01, 125.13, 123.94, 122.88 (Ar-C), 52.37 (CH_2), 27.01 (CH_2), 20.89 (CH_3), 18.13 (CH_3); (ESI-MS) m/z 615.3 $(M + H)^+$; Anal. Calcd for $C_{29}H_{24}ClN_9OS_2$: C, 56.72; H, 3.94; N, 20.53; Found: C, 56.70; H, 3.93; N, 20.52%.

- **(E)-2-(4-(((5-(benzo[d]thiazol-2-yl)-4-((4-chlorobenzylidene)amino)-4H-1,2,4-triazol-3-yl)thio)methyl)-1H-1,2,3-triazol-1-yl)-N-mesitylacetamide (10b)**

  Yield 86%; Reddish orange; mp 231-233 °C; FT-IR (KBr, ν, cm^{-1}): 3232.80 (NH Stretch), 1658.84 (amide Stretch); ^{1}H NMR (400 MHz, DMSO) δ 9.65 (s, 1H, NH), 9.24 (s, 1H, HC=N), 8.21 (m, 1H, Ar-H), 8.13 (s, 1H, CH, Ar-H), 7.98–7.96 (d, *J* = 8.2 Hz, 2H, Ar-H), 7.86 (m, 1H, Ar-H), 7.70–7.68 (d, *J* = 8.2 Hz, 2H, Ar-H), 7.54 (dq, *J* = 7.5, 4.1 Hz, 2H, Ar-H), 6.83 (s, 1H, Ar-H), 5.33 (s, 2H, CH_2), 4.66 (s, 2H, CH_2), 2.19 (s, 3H, CH_3), 2.07 (s, 6H, C_2H_6); ^{13}C NMR (101 MHz, DMSO) δ 131.36 (HC=N), 130.07, 128.77, 127.46, 127.19, 125.93, 123.95, 122.89 (Ar-C), 52.12 (CH_2), 26.94 (CH_2), 20.93 (CH_3), 18.38 (C_2H_6); (ESI-MS) m/z 628.3 $(M + H)^+$; Anal. Calcd for $C_{30}H_{26}ClN_9OS_2$: C, 57.36; H, 4.17; N, 20.07; Found: C, 57.34; H, 4.15; N, 20.06%.

- **(E)-2-(4-(((5-(benzo[d]thiazol-2-yl)-4-((4-chlorobenzylidene)amino)-4H-1,2,4-triazol-3-yl)thio)methyl)-1H-1,2,3-triazol-1-yl)-N-(2,6-difluorophenyl)acetamide (10c)**

  Yield 81%; Reddish orange; mp 232-234 °C; FT-IR (KBr, ν, cm^{-1}): 3232.80 (NH Stretch), 1689.70 (amide Stretch); ^{1}H NMR (400 MHz, DMSO) δ 10.28 (s, 1H, NH), 9.25 (s, 1H, HC=N), 8.22–8.19 (dt, *J* = 6.2, 3.4 Hz, 1H, Ar-H), 8.15 (s, 1H, CH, Ar-H), 7.99–7.97 (d, *J* = 8.4 Hz, 2H, Ar-H), 7.86–7.84 (dt, *J* = 7.1, 3.6 Hz, 1H,, Ar-H), 7.70–7.63 (d, *J* = 8.4 Hz, 2H, Ar-H), 7.54–7.52 (dt, *J* = 6.1, 3.6 Hz, 2H, Ar-H), 7.39–7.32 (ddd, *J* = 14.6, 8.5, 6.3 Hz, 1H,Ar-H), 7.17–7.13 (t, *J* = 8.2 Hz, 2H), 5.43 (s, 2H, CH_2), 4.66 (s, 2H, CH_2); ^{13}C NMR (101 MHz, DMSO) δ 131.35 (HC=N), 130.06, 128.93, 128.83, 128.74, 127.44, 127.17, 126.09, 124.64, 123.94, 122.88, 112.52, 112.48, 112.30 (Ar-C), 51.85 (CH_2), 26.88 (CH_2); (ESI-MS) m/z 622.4 $(M + H)^+$; Anal. Calcd for $C_{27}H_{18}ClF_2N_9OS_2$: C, 52.13; H, 2.92; N, 20.27; Found: C, 52.10; H, 2.90; N, 20.25%.

- **(E)-2-(4-(((5-(benzo[d]thiazol-2-yl)-4-((4-chlorobenzylidene)amino)-4H-1,2,4-triazol-3-yl)thio)methyl)-1H-1,2,3-triazol-1-yl)-N-(2,6-dimethylphenyl)acetamide (10d)**

  Yield 91%; Reddish orange; mp 222-224 °C; FT-IR (KBr, ν, cm^{-1}): 3240.52 (NH Stretch), 1666.55 (amide Stretch); ^{1}H NMR (400 MHz, DMSO) δ 9.75 (s, 1H, NH),

9.25 (s, 1H, HC=N)), 8.21–8.19 (dt, *J* = 6.2, 3.8 Hz, 1H, Ar-H), 8.15 (s, 1H, CH, Ar-H), 7.98–7.96 (d, *J* = 8.2 Hz, 2H,Ar-H), 7.87–7.84 (dt, *J* = 7.1, 3.5 Hz, 1H), 7.70–7.68 (d, *J* = 8.3 Hz, 2H, Ar-H), 7.54–7.52 (dt, *J* = 6.1, 3.6 Hz, 2H, Ar-H), 7.09–7.02 (q, *J* = 4.8 Hz, 3H, Ar-H), 5.36 (s, 2H, CH_2), 4.67 (s, 2H, CH_2), 2.12 (s, 6H, C_2H_6); ^{13}C NMR (101 MHz, DMSO) δ 131.35 (HC=N), 130.07, 128.19, 127.45, 127.19, 125.97, 123.95, 122.89 (Ar-C), 52.11 (CH_2), 26.89 (CH_2), 18.47 (C_2H_6); (ESI-MS) m/z 614.3 $(M + H)^+$; Anal. Calcd for $C_{29}H_{24}ClN_9OS_2$: C, 56.72; H, 3.94; N, 20.53; Found: C, 56.71; H, 3.90; N, 20.50%.

- **(E)-2-(4-(((5-(benzo[d]thiazol-2-yl)-4-((4-chlorobenzylidene)amino)-4H-1,2,4-triazol-3-yl)thio)methyl)-1H-1,2,3-triazol-1-yl)-N-(4-fluorophenyl)acetamide (10e)**

  Yield 89%; Reddish orange; mp 214-216 °C; FT-IR (KBr, ν, cm^{-1}): 3348.54 (NH Stretch), 1689.70 (amide Stretch); ^1H NMR (400 MHz, DMSO) δ 10.52 (s, 1H, NH), 9.20 (s, 1H, HC=N), 8.20 (s, 2H, Ar-H), 8.13 (s, 1H, CH, Ar-H), 7.97 (s, 2H, Ar-H), 7.85 (s, 1H, Ar-H), 7.69 (s, 2H, Ar-H), 7.53 (s, 4H, Ar-H), 7.08 (s, 2H, Ar-H), 5.32 (s, 2H, CH_2), 4.68 (s, 2H, CH_2); ^{13}C NMR (101 MHz, DMSO) δ 169.92 (C=O), 164.55 (C-F), 159.83 (C-S), 157.44 (C=N), 154.74, 153.00, 151.10, 145.83, 142.76, 138.68, 135.24, 134.62, 131.34, 130.74, 130.06, 127.45, 127.17, 126.07, 123.95, 122.89 (Ar-C), 121.38 (d, *J* = 7.9 Hz, Ar-C), 115.90 (d, *J* = 22.1 Hz, Ar-C), 52.60 (CH_2), 27.12 (CH_2); (ESI-MS) m/z 604.1 $(M + H)^+$; Anal. Calcd for $C_{27}H_{19}ClFN_9OS_2$: C, 53.68; H, 3.17; N, 20.87; Found: C, 53.64; H, 3.16; N, 20.83%.

- **(E)-2-(4-(((5-(benzo[d]thiazol-2-yl)-4-((4-chlorobenzylidene)amino)-4H-1,2,4-triazol-3-yl)thio)methyl)-1H-1,2,3-triazol-1-yl)-N-(4-chlorophenyl)acetamide (10f)**

  Yield 86%; Reddish orange; mp 235-237 °C; FT-IR (KBr, ν, cm^{-1}): 3333.10 (NH Stretch), 1681.98 (amide Stretch); ^1H NMR (400 MHz, DMSO) δ 10.59 (s, 1H, NH), 9.19 (s, 1H, HC=N), 8.27–8.20 (m, 1H, Ar-H), 8.11 (s, 1H, CH, Ar-H), 7.98–7.97 (d, *J* = 6.3 Hz, 2H, Ar-H), 7.87–7.84 (m, 1H, Ar-H), 7.70–7.69 (d, *J* = 6.2 Hz, 2H, Ar-H), 7.54– 7.52 (d, *J* = 10.4 Hz, 4H, Ar-H), 7.29–7.27 (d, *J* = 10.4 Hz, 2H, Ar-H), 5.33 (s, 2H, CH_2), 4.66 (s, 2H, CH_2); ^{13}C NMR (101 MHz, DMSO) δ 169.98

(C=O), 164.79 (C-S), 154.70 (C=N), 152.97, 151.01, 145.80, 142.75, 138.69, 137.76, 134.60, 131.36, 130.75, 130.08, 129.21, 127.75, 127.44, 127.15, 126.03, 123.95, 122.88, 121.13 (Ar-C), 52.65 (CH_2), 27.14 (CH_2); (ESI-MS) m/z 620.2 $(M + H)^+$; Anal. Calcd for $C_{27}H_{19}Cl_2N_9OS_2$: C, 52.26; H, 3.09; N, 20.32; Found: C, 52.25; H, 3.09; N, 20.30%.

- **(E)-2-(4-(((5-(benzo[d]thiazol-2-yl)-4-((4-chlorobenzylidene)amino)-4H-1,2,4-triazol-3-yl)thio)methyl)-1H-1,2,3-triazol-1-yl)-N-(4-bromophenyl)acetamide (10g)**

  Yield 84%; Reddish orange; mp 213-215 °C; FT-IR (KBr, ν, cm^{-1}): 3333.10 (NH Stretch), 1681.98 (amide Stretch); ^1H NMR (400 MHz, DMSO) δ 10.58 (s, 1H, NH), 9.19 (s, 1H, HC=N), 8.22–8.20 (dq, *J* = 7.2, 4.0 Hz, 1H, Ar-H), 8.11 (s, 1H, CH, Ar-H), 7.99–7.96 (m, 2H, Ar-H), 7.87–7.85 (dq, *J* = 7.4, 4.0 Hz, 1H, Ar-H), 7.71–7.63 (m, 2H, Ar-H), 7.55–7.53 (m, 3H, Ar-H), 7.48–7.39 (m, 3H, Ar-H), 5.32 (s, 2H, CH_2), 4.66 (s, 2H, CH_2); ^{13}C NMR (101 MHz, DMSO) δ 132.13 (HC=N), 131.35, 130.08, 127.46, 127.18, 126.07, 123.96, 122.91, 121.49 (Ar-C), 52.67 (CH_2), 27.15 (CH_2); (ESI-MS) m/z 664.2 $(M + H)^+$; Anal. Calcd for $C_{27}H_{19}BrClN_9OS_2$: C, 48.77; H, 2.88; N, 18.96; Found: C, 48.77; H, 2.86; N, 18.92%.

- **(E)-2-(4-(((5-(benzo[d]thiazol-2-yl)-4-((4-chlorobenzylidene)amino)-4H-1,2,4-triazol-3-yl)thio)methyl)-1H-1,2,3-triazol-1-yl)-N-(3-chlorophenyl)acetamide (10h)**

  Yield 85%; Reddish orange; mp 196-198 °C; FT-IR (KBr, ν, cm^{-1}): 3348.54 (NH Stretch), 1689.70 (amide Stretch); ^1H NMR (400 MHz, DMSO) δ 10.67 (s, 1H, NH), 9.24 (s, 1H, HC=N), 8.24–8.17 (m, 2H, Ar-H), 7.99–7.97 (d, *J* = 7.8 Hz, 2H, Ar-H), 7.85 (m, 1H, Ar-H), 7.75 (s, 1H, Ar-H), 7.69–7.67(d, *J* = 8.1 Hz, 2H, Ar-H), 7.53–7.51 (m, 2H, Ar-H), 7.42–7.40 (d, *J* = 8.1 Hz, 1H), 7.32–7.28 (dt, *J* = 15.9, 7.8 Hz, 1H, Ar-H), 7.12–7.11 (d, *J* = 8.0 Hz, 1H, Ar-H), 5.36 (s, 2H, CH_2), 4.6 (s, 2H, CH_2); ^{13}C NMR (101 MHz, DMSO) δ 169.73 (C=O), 165.07 (C-S), 154.70 (C=N), 152.98, 151.24, 145.82, 142.82, 140.26, 138.69, 134.61, 133.67, 131.34, 131.03, 130.74, 130.04, 127.41, 127.15, 126.07, 123.94, 122.84, 119.18, 118.05

(Ar-C), 52.70 (CH_2), 27.00 (CH_2); (ESI-MS) m/z 620.2 $(M + H)^+$; Anal. Calcd for $C_{27}H_{19}Cl_2N_9OS_2$: C, 52.26; H, 3.09; N, 20.32; Found: C, 52.23; H, 3.07; N, 20.32%.

- **(E)-2-(4-(((5-(benzo[d]thiazol-2-yl)-4-((4-chlorobenzylidene)amino)-4H-1,2,4-triazol-3-yl)thio)methyl)-1H-1,2,3-triazol-1-yl)-N-(p-tolyl)acetamide (10i)**

  Yield 94%; Reddish orange; mp 234-236 °C; FT-IR (KBr, ν, cm^{-1}): 3286.81 (NH Stretch), 1674.27 (amide Stretch); ^1H NMR (400 MHz, DMSO) δ 10.36 (s, 1H, NH), 9.20 (s, 1H, HC=N), 8.21–8.19 (dq, *J* = 7.2, 3.9 Hz, 1H, Ar-H), 8.11 (s, 1H, CH, Ar-H), 7.98–7.96 (d, *J* = 8.5 Hz, 2H, Ar-H), 7.87–7.84 (dq, *J* = 7.2, 3.9 Hz, 1H, Ar-H), 7.70–7.64 (d, *J* = 8.3 Hz, 2H, Ar-H), 7.55–7.51 (dt, *J* = 6.1, 3.6 Hz, 2H, Ar-H), 7.44–7.40 (d, *J* = 8.1 Hz, 2H, Ar-H), 7.07–7.04 (d, *J* = 8.1 Hz, 2H, Ar-H), 5.29 (s, 2H, CH_2), 4.66 (s, 2H, CH_2), 2.22 (s, 3H, CH_3); ^{13}C NMR (101 MHz, DMSO) δ 169.92 (C=O), 164.31 (C-S), 154.73 (C=N), 153.01, 151.08, 145.83, 142.75, 138.67, 136.32, 134.63, 133.13, 131.34, 130.75, 130.06, 129.67, 127.97, 127.44, 127.16, 126.03, 123.96, 122.88, 119.59 (Ar-C), 52.65 (CH_2), 27.15 (CH_2), 20.88 (CH_3); (ESI-MS) m/z 600.2 $(M + H)^+$; Anal. Calcd for $C_{28}H_{22}ClN_9OS_2$: C, 56.04; H, 3.70; N, 21.01; Found: C, 56.03; H, 3.69; N, 21.00%.

- **(E)-2-(4-(((5-(benzo[d]thiazol-2-yl)-4-((4-chlorobenzylidene)amino)-4H-1,2,4-triazol-3-yl)thio)methyl)-1H-1,2,3-triazol-1-yl)-N-(4-methoxyphenyl)acetamide (10j)**

  Yield 90%; Reddish orange; mp 198-200 °C; FT-IR (KBr, ν, cm^{-1}): 3271.38 (NH Stretch), 1674.27 (amide Stretch); ^1H NMR (400 MHz, DMSO) δ 10.31 (s, 1H, NH), 9.19 (s, 1H, HC=N), 8.21–8.20 (m, 1H, Ar-H), 8.10 (s, 1H, CH, Ar-H), 7.98–7.96 (d, *J* = 8.3 Hz, 2H, Ar-H), 7.86–7.85 (dd, *J* = 6.1, 3.3 Hz, 1H, Ar-H), 7.71–7.62 (d, *J* = 8.2 Hz, 2H, Ar-H), 7.55–7.53 (dd, *J* = 6.2, 3.2 Hz, 2H, Ar-H), 7.46–7.40 (d, *J* = 8.5 Hz, 2H, Ar-H), 6.85–6.80 (d, *J* = 8.6 Hz, 2H, Ar-H), 5.27 (s, 2H, CH_2), 4.66 (s, 2H, CH_2), 3.69 (s, 2H, OCH_3); ^{13}C NMR (101 MHz, DMSO) δ 131.35 (HC=N), 130.07, 127.46, 127.18, 126.04, 124.65, 123.96, 122.90, 121.08, 114.38 (Ar-C), 55.60 (O-CH_3), 52.59 (CH_2), 27.18 (CH_2); (ESI-MS) m/z 616.3 $(M + H)^+$; Anal. Calcd for $C_{28}H_{22}ClN_9O_2S_2$: C, 54.59; H, 3.60; N, 20.46; Found: C, 54.55; H, 3.57; N, 20.45%.

5.3.2 *In vitro* alpha amylase inhibition procedure

The ability of the synthesized benzothiazole-based compounds to inhibit the α-amylase enzyme was evaluated to determine their potential as antidiabetic agents. To perform the α-amylase inhibition assay, a microplate-based method was utilized and followed a well-established protocol.[273] To obtain a stock concentration of 1 mg/mL, 1 mg of each compound was first dissolved in 100 µL of DMSO, and then 900 µL of double-distilled water was added. A 96-well plate was used to prepare the highest concentration (400 µg/mL) by transferring 100 µL of each sample from this stock. Subsequently, the concentration was serially diluted using 50 µL of freshly prepared sodium phosphate (NaP) buffer to obtain concentrations of 400 µg/mL, 200 µg/mL, 100 µg/mL, 50 µg/mL, 25 µg/mL, and 12.5 µg/mL. The diluted samples in each well were supplemented with 50 µL of α-amylase enzyme (0.5 mg/mL in NaP buffer), and incubated for 30 minutes at room temperature. Then, the enzymatic reaction was started by adding 50 µL of a freshly made 1% starch solution in NaP buffer. Following a 10-minute incubation, the reaction was halted by adding 50 µL of newly prepared DNS reagent. The plate was subsequently immersed in a boiling water bath (90-95°C) for 8 minutes, causing the expected transition from yellow to orange. This color alteration confirmed the existence of reducing sugars produced by α-amylase. Using a microplate reader, absorbance readings at 540 nm were recorded. To adjust for background absorbance, a color blank was made for each concentration of the test sample, with all reagents added except α-amylase. The enzyme's activity on starch led to the formation of reducing sugars, which was reflected in the observed absorbance. To calculate the percentage inhibition of α-amylase activity, the corrected absorbance values were derived by subtracting the blank's OD from the sample's average OD, using the formula provided.

$$\%Inhibition\ (I\%) = \left(\frac{Ac - As}{Ac}\right) \times 100$$

where As is the average absorbance of the sample, and Ac is the average absorbance of the control (without the test compound). Acarbose, a known α-amylase inhibitor, was used as the positive control in similar concentrations for comparison. The IC_{50} values were calculated by correlating the percentage inhibition with the logarithmic concentrations of the compounds. Linear regression analysis was performed using the equation Y=MX+C, where Y=50, and M and C values were derived from the inhibition curve.

5.3.3 *In vitro* alpha glucosidase inhibition procedure

In order to evaluate their potential as antidiabetic agents, the synthesized benzothiazole-based compounds were subjected to assessment of their alpha-glucosidase inhibitory activity using a microplate-based method.[273] The process began by dissolving 1 mg of each compound separately in 100 µL of DMSO. Then, 900 µL of double-distilled water was introduced to the mixture, resulting in a final stock concentration of 1 mg/mL. The transfer of 100 µL of the highest concentration (400 µg/mL) was carried out from this stock to a 96-well plate. Serial dilutions of the compounds were prepared using 50 µL of freshly prepared sodium phosphate (NaP) buffer (0.02 M, pH 6.8-7.0), resulting in final concentrations of 400 µg/mL, 200 µg/mL, 100 µg/mL, 50 µg/mL, 25 µg/mL, and 12.5 µg/mL. The sample dilutions were treated by adding 50 µL of alpha-glucosidase enzyme, which had been prepared in NaP buffer at a concentration of 0.5 U/mL. Following the addition, the reaction mixture was incubated for 20 minutes at a temperature of 37°C. Once the incubation period was completed, the wells were each supplemented with 50 µL of the substrate p-nitrophenyl-α-D-glucopyranoside (PNPG) at a concentration of 3 mM. The reaction could then progress for a duration of 10 minutes at a temperature of 37°C. The reaction was then terminated by the addition of 150 µL of 0.1 M sodium carbonate (Na_2CO_3) to each well. The absorbance at 405 nm was measured using a microplate reader to monitor the formation of a yellow-colored product. In order to compensate for any non-specific absorbance, a color blank was created for each concentration by excluding the alpha-glucosidase enzyme. The calculation of the percentage inhibition of alpha-glucosidase was done by applying the formula provided below.

$$\%Inhibition\ (I\%) = \left(\frac{Ac - As}{Ac}\right) \times 100$$

where As is the average absorbance of the sample, and Ac is the average absorbance of the control (without the test compound). Acarbose, a known alpha-glucosidase inhibitor, was used as a positive control for comparison. The determination of the IC50 values involved plotting the percentage inhibition against the logarithmic concentrations of the compounds. The linear regression equation Y=MX+C was used, where Y=50, and M and C values were derived from the inhibition curve.

5.3.4 *In vitro* Anticancer Single dose assay procedure

The synthesized compounds were subjected to a one-dose screening assay in the NCI DTP-60 program in order to evaluate their potential as anticancer agents. [198,199,200] The testing process involved evaluating each compound against around 60 human cancer cell lines that encompassed different types of cancer. A concentration of 10 μM was utilized for this purpose. In order to reach the desired concentration, the compounds were carefully prepared by dissolving them in a solution consisting of a mixture of DMSO and glycerol, with a ratio of 9 parts DMSO to 1 part glycerol. The cell lines were cultured by seeding them into 96-well plates and allowing them to adhere overnight, following the standard protocols. Following that, the test compound was added to each well and left to incubate for a period of 48 hours. Following the incubation period, an examination of cell viability was performed by utilizing an appropriate assay, such as sulforhodamine B (SRB). This particular assay measures total protein content or metabolic activity, serving as an indicator for both cell growth and viability. To determine the percentage of cell growth inhibition, the untreated controls were compared to the treated wells. The utilization of this approach allowed for the identification of impacts that not only inhibit growth but also exhibit cytotoxic properties. Compounds that exhibit notable growth suppression during this stage have the potential to be regarded as prospective candidates for further investigation as anti-cancer agents.

5.4 Conclusion

In this study, a series of benzothiazole-based 1,2,4-triazole and 1,2,3-triazole derivatives were synthesized and fully characterized. The α-amylase and α-glucosidase inhibition profiles of the compounds revealed moderate antidiabetic activity. On the other hand, the results regarding their potential as anticancer agents were particularly encouraging, as a number of compounds exhibited strong cytotoxic effects on various cancer cell lines, such as melanoma, ovarian, CNS, and breast cancers. The NCI chose to advance all compounds to further five-dose studies as a result of their remarkable performance in the one-dose screening. The results of this study highlight the immense potential of benzothiazole-triazole hybrids as highly promising candidates for further

research and development, specifically in the field of anticancer agents. Additionally, these findings shed light on their moderate efficacy in the realm of antidiabetic therapy.

5.5 Spectral data

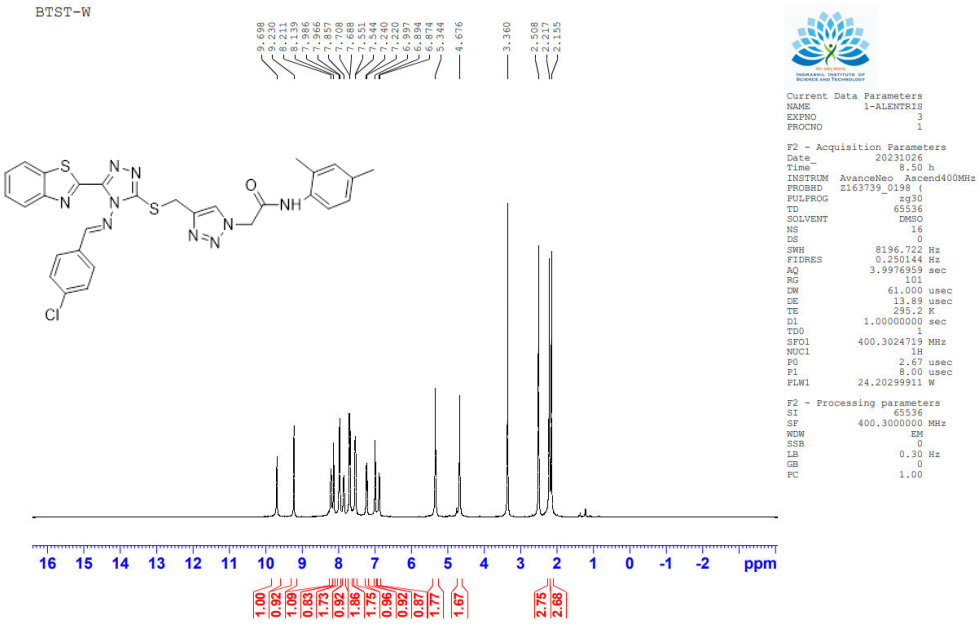

Figure 13: Representative ^{1}H NMR spectrum of compound 10a

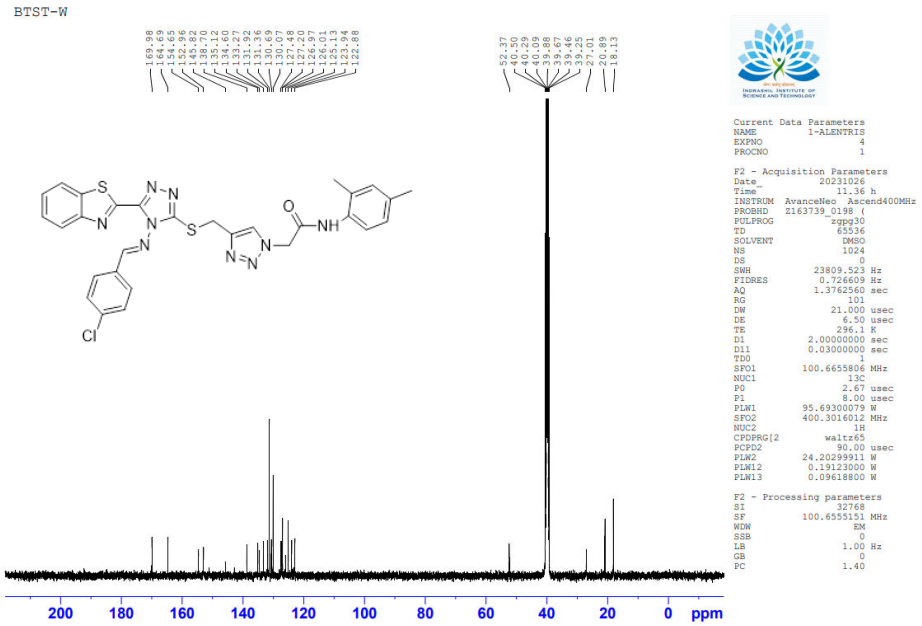

Figure 14: Representative ^{13}C NMR spectrum of compound 10a

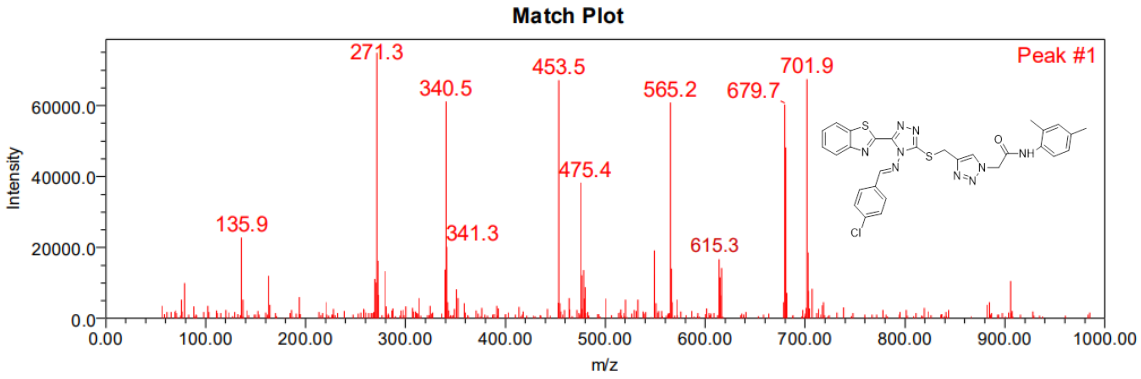

Figure 15: Representative mass spectrum of compound 10a

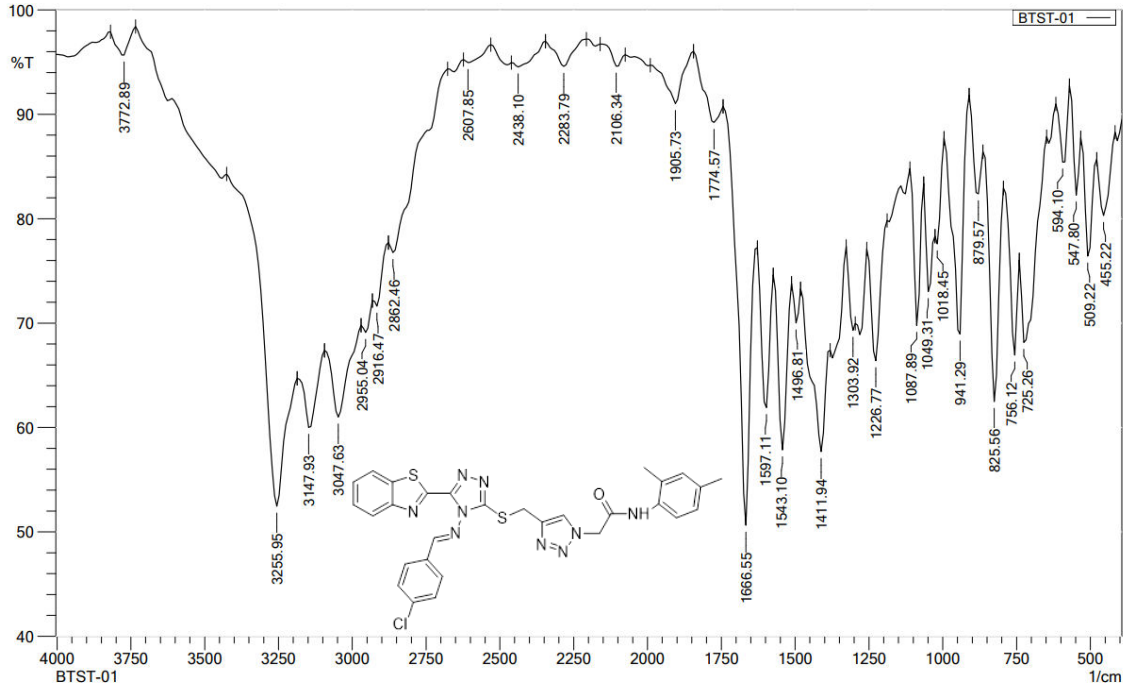

Figure 16: Representative FT-IR spectrum of compound 10a

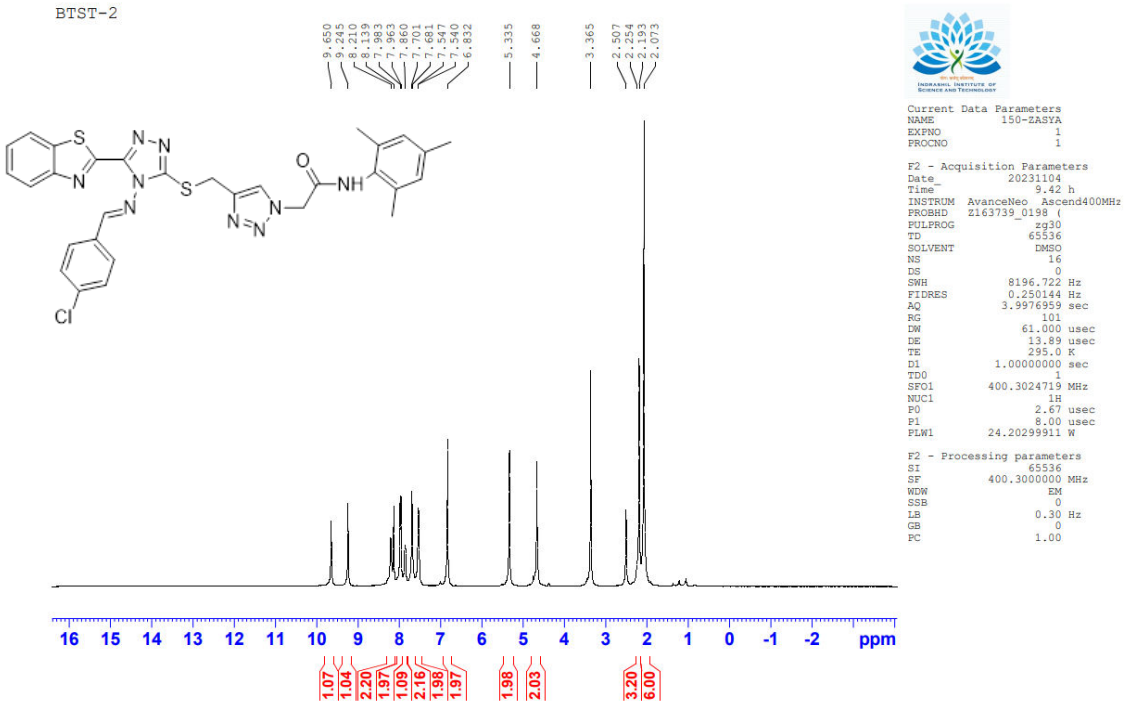

Figure 17: Representative ^{1}H NMR spectrum of compound 10b

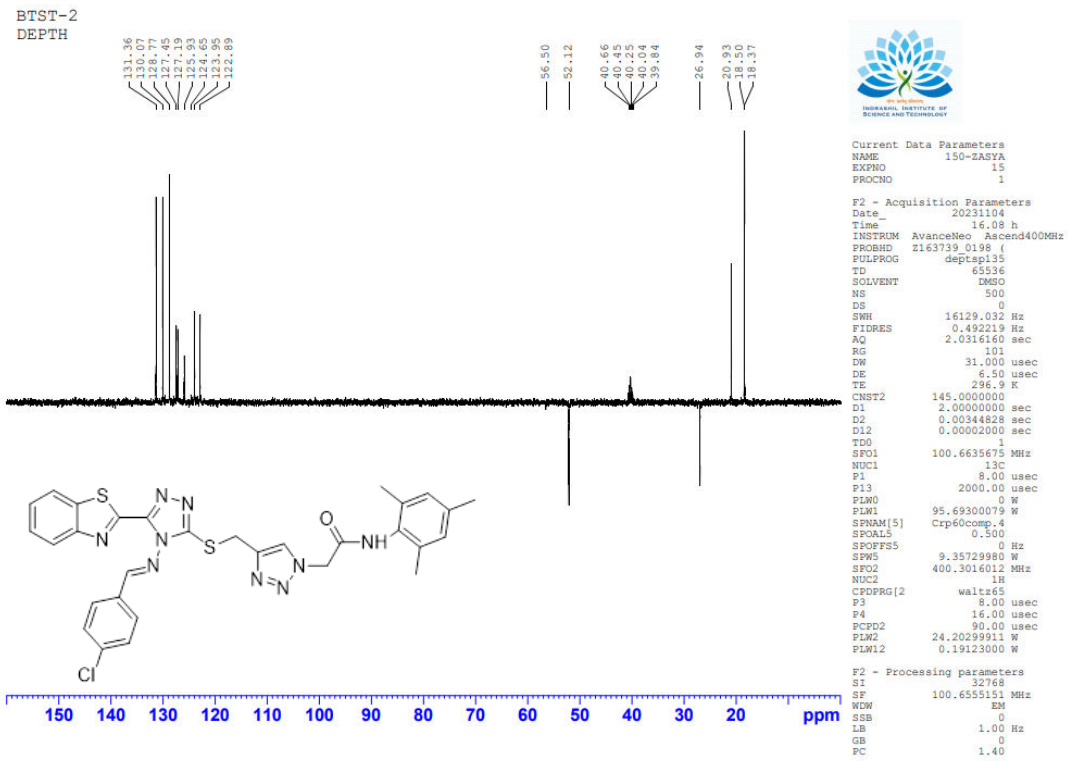

Figure 18: Representative ^{13}C DEPT-135 NMR spectrum of compound 10b

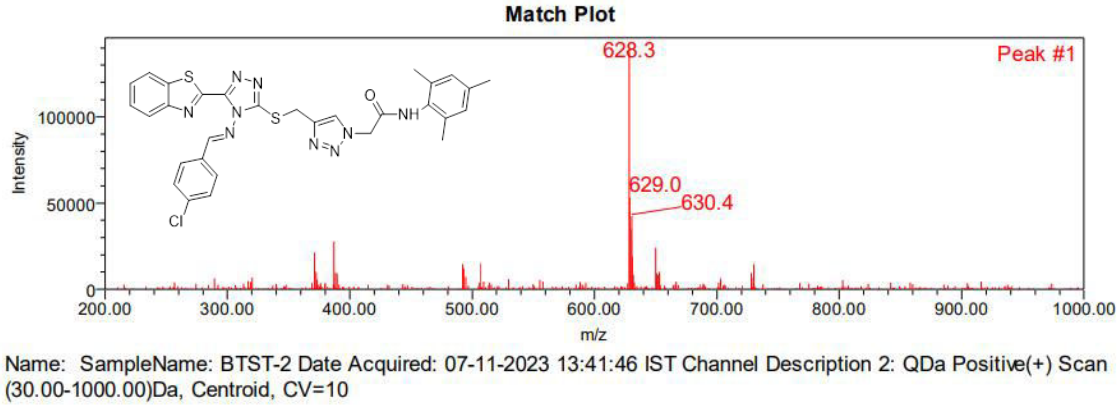

Figure 19: Representative mass spectrum of compound 10b

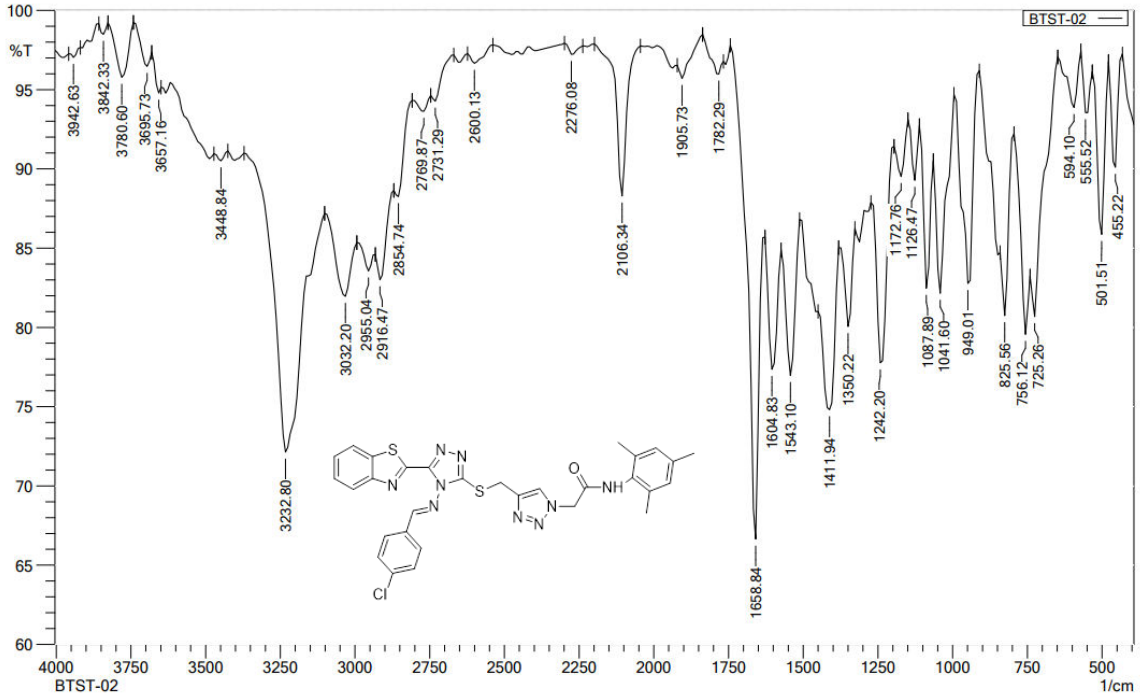

Figure 20: Representative FT-IR spectrum of compound 10b

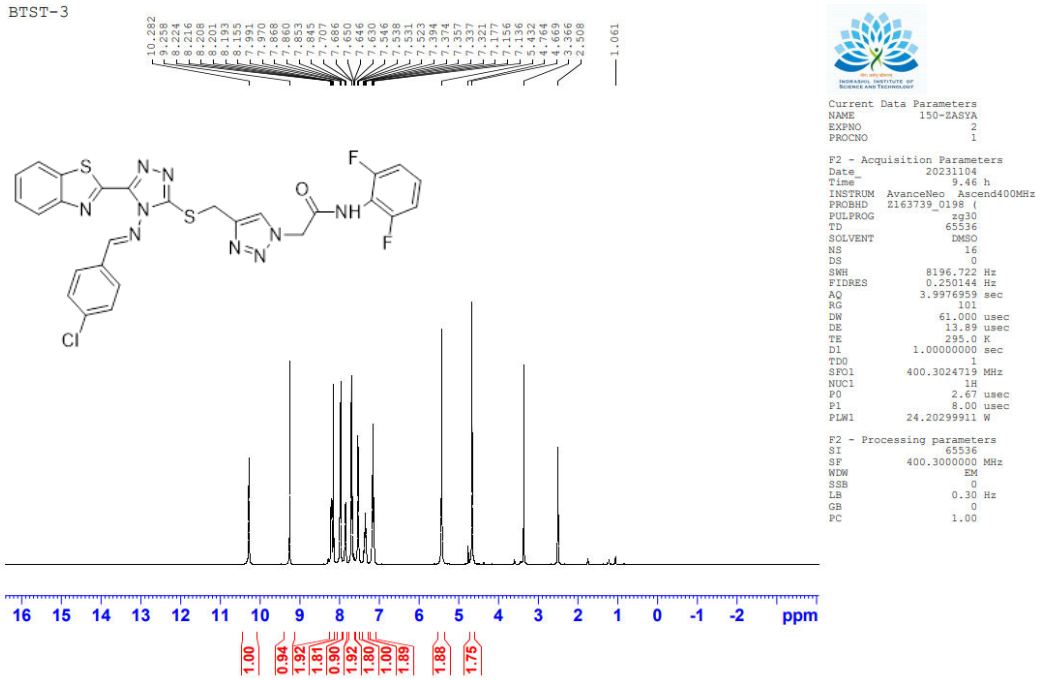

Figure 21: Representative ^{1}H NMR spectrum of compound 10c

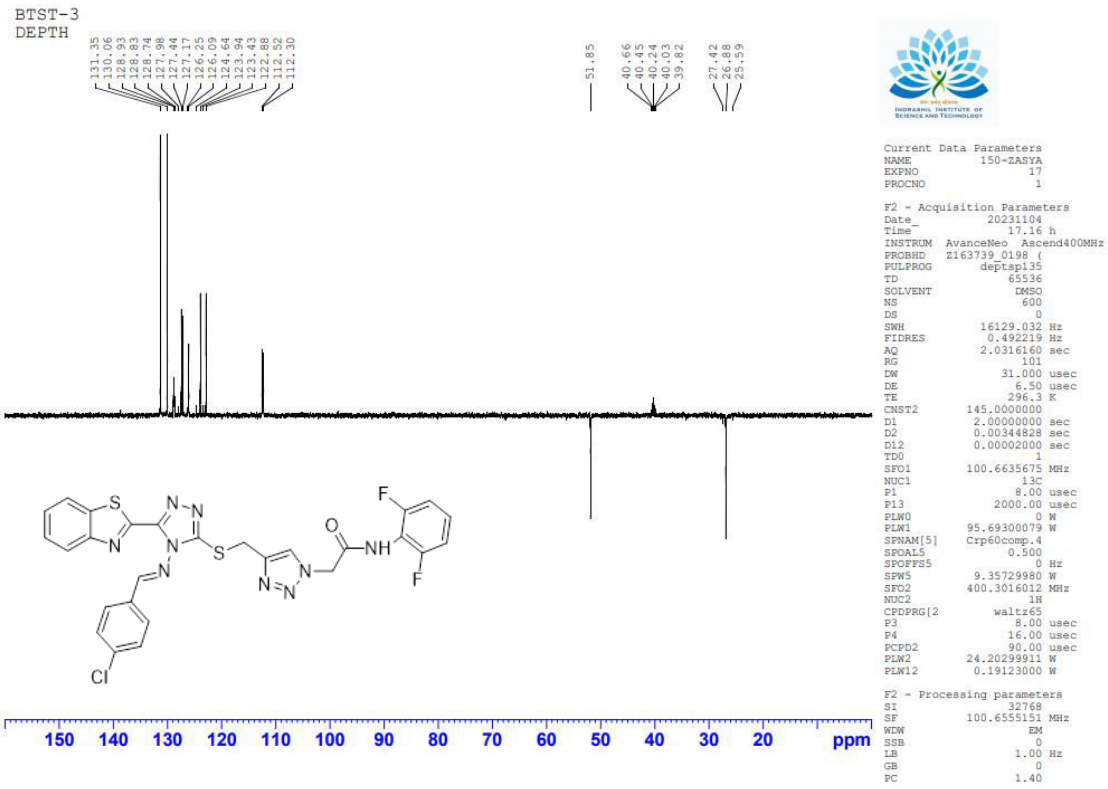

Figure 22: Representative ^{13}C DEPT-135 NMR spectrum of compound 10c

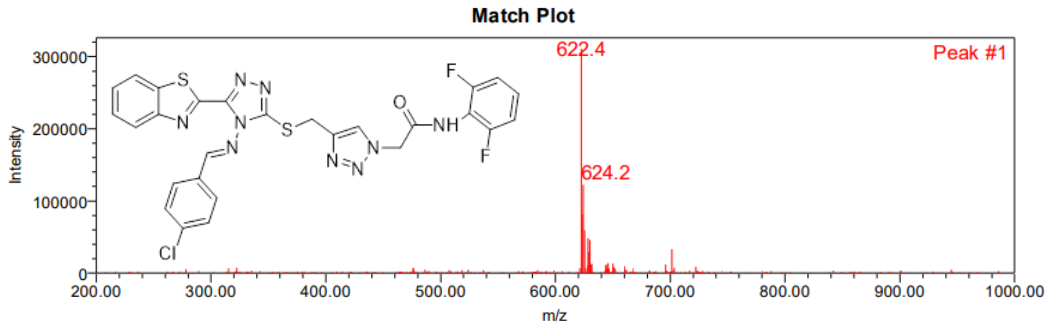

Figure 23: Representative mass spectrum of compound 10c

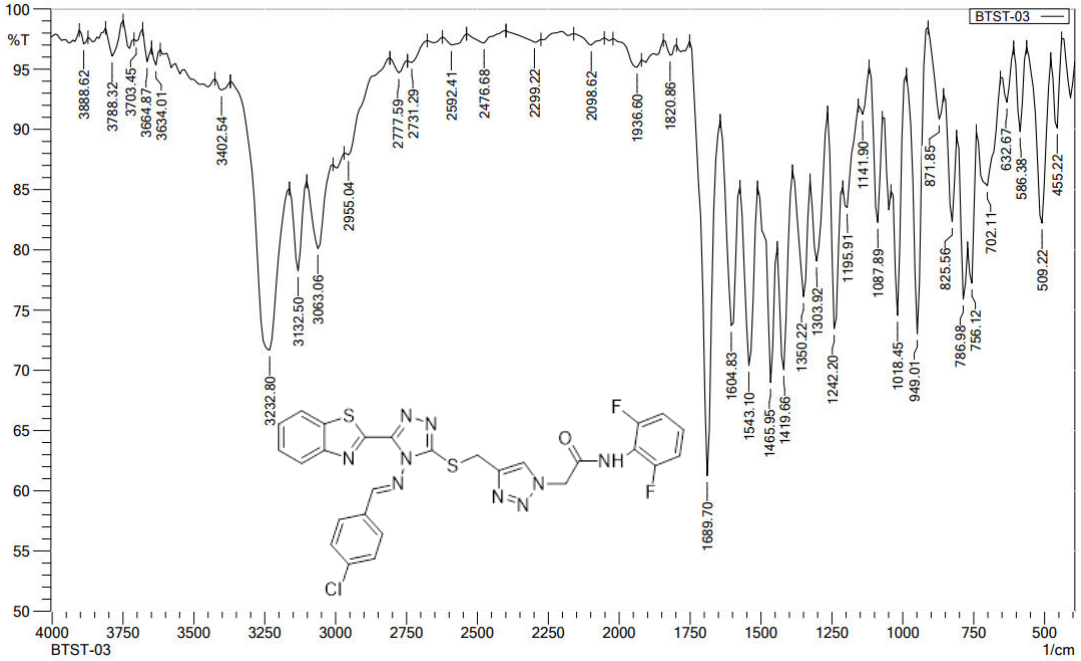

Figure 24: Representative FT-IR spectrum of compound 10c

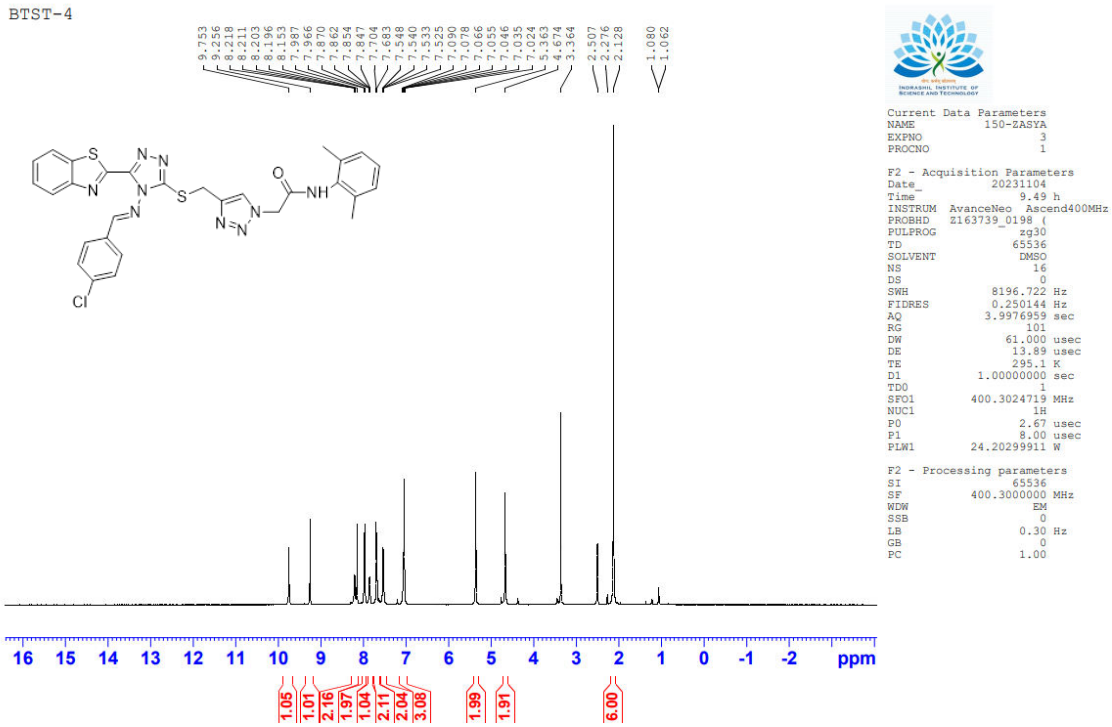

Figure 25: Representative ^{1}H NMR spectrum of compound 10d

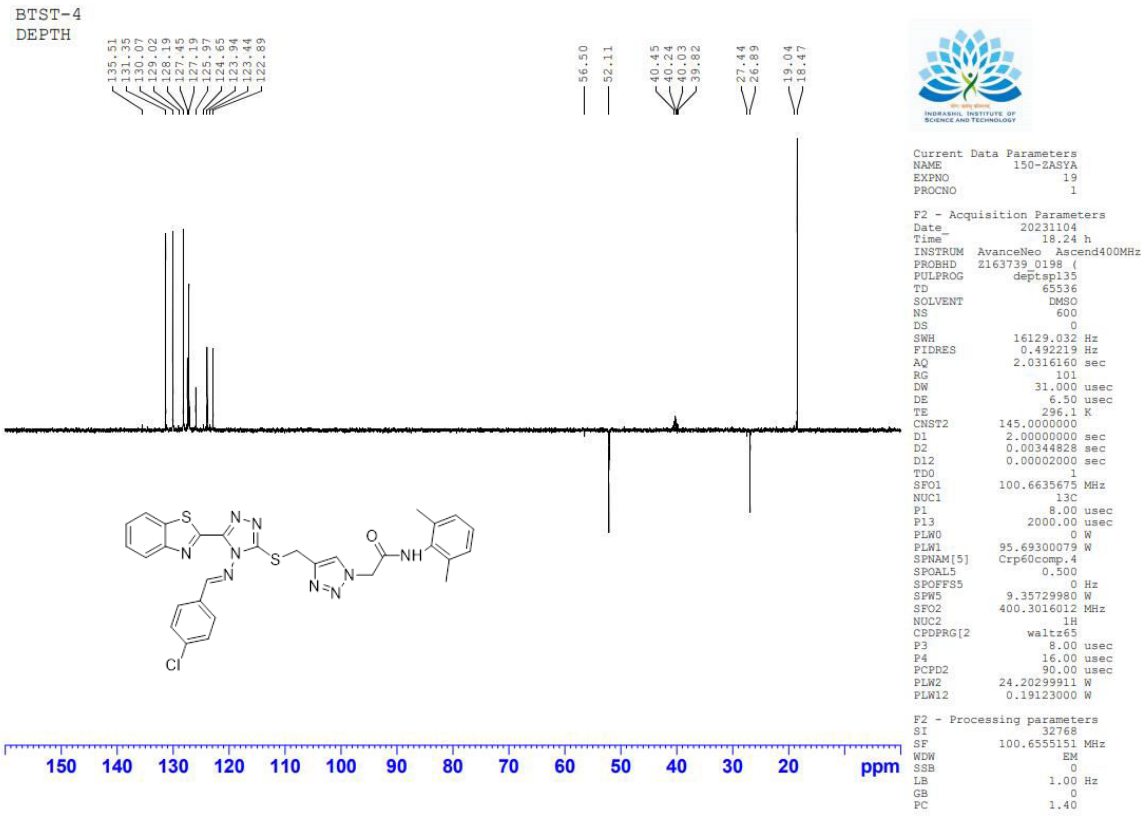

Figure 26: Representative ^{13}C DEPT-135 NMR spectrum of compound 10d

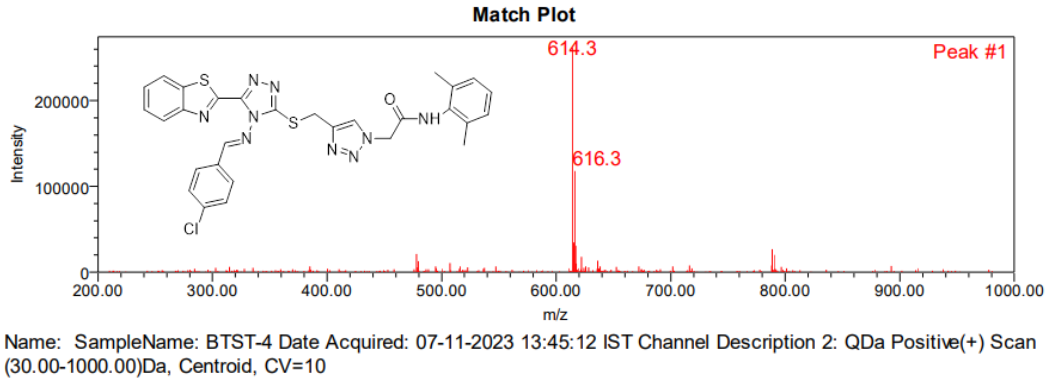

Figure 27: Representative mass spectrum of compound 10d

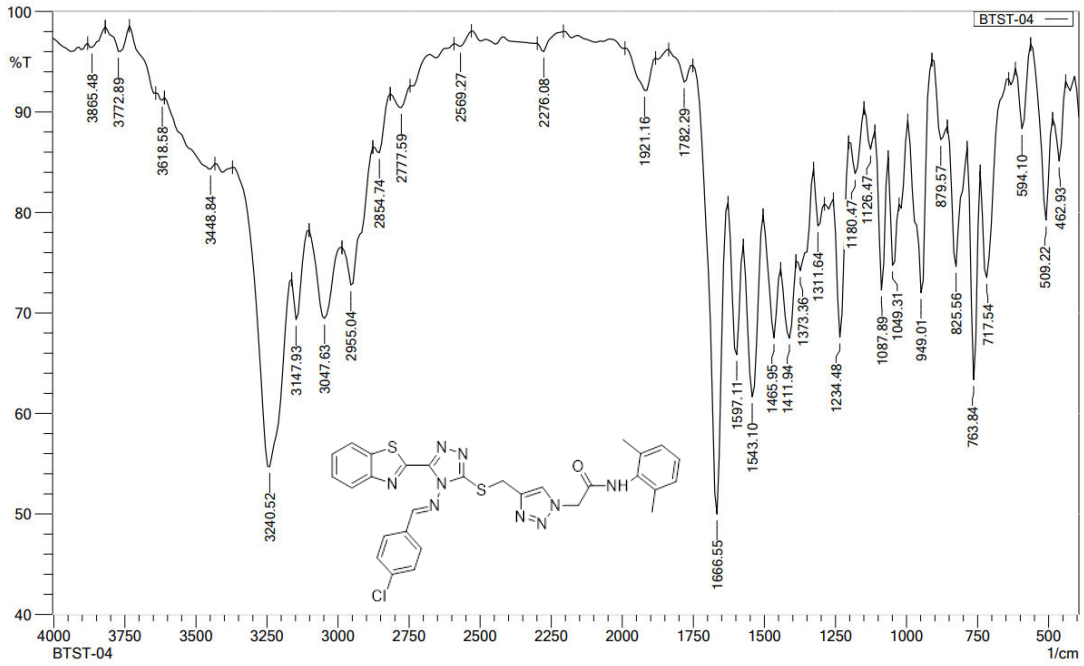

Figure 28: Representative FT-IR spectrum of compound 10d

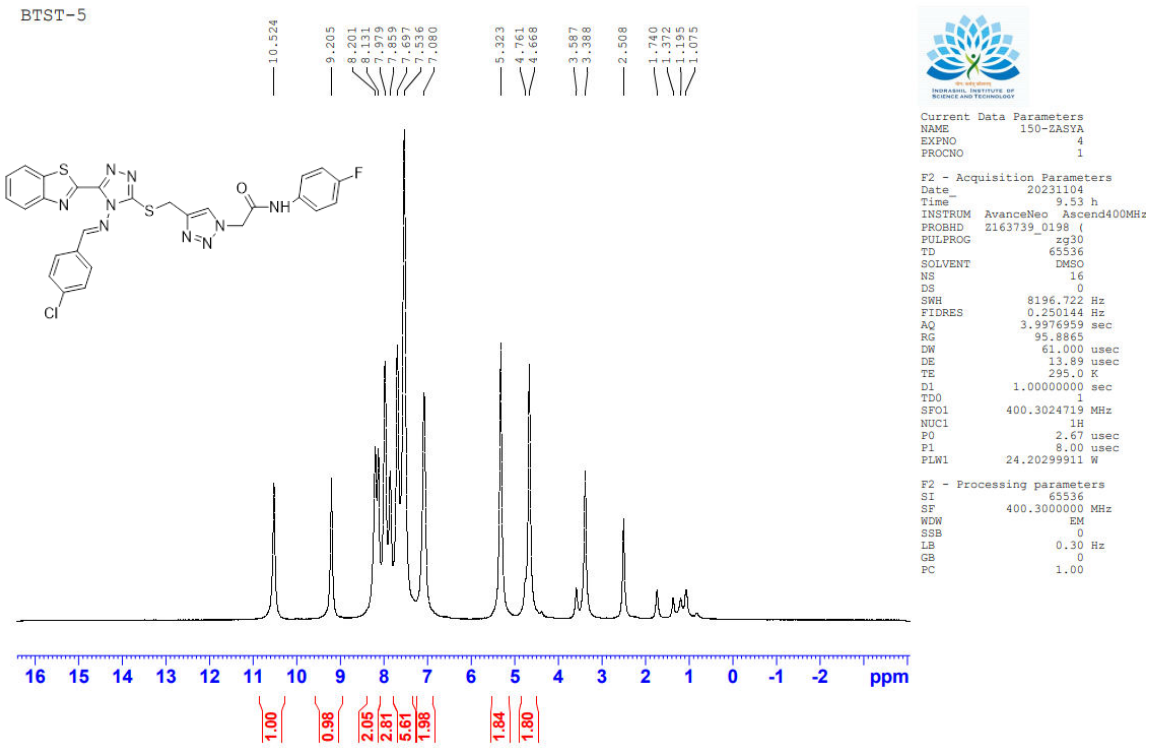

Figure 29: Representative ^{1}H NMR spectrum of compound 10e

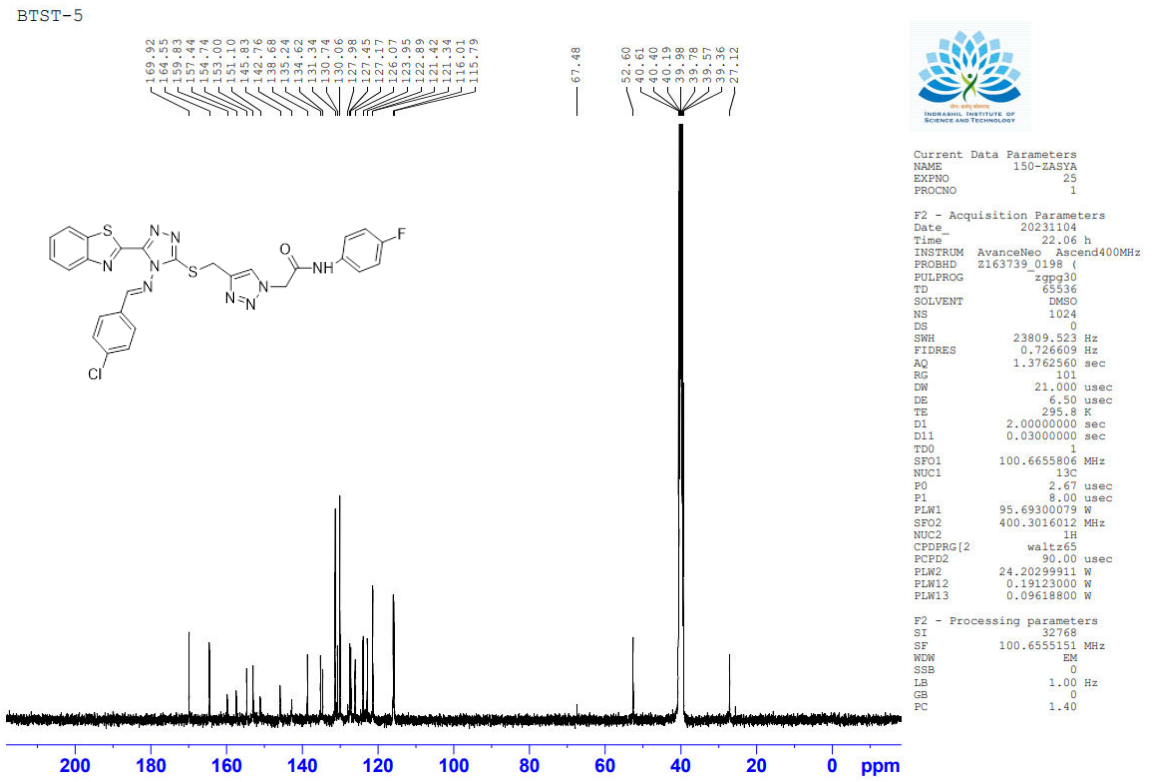

Figure 30: Representative ^{13}C NMR spectrum of compound 10e

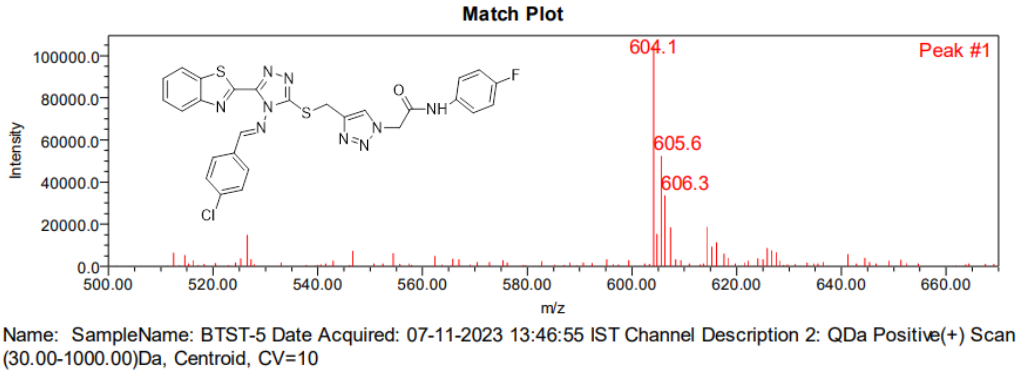

Figure 31: Representative mass spectrum of compound 10e

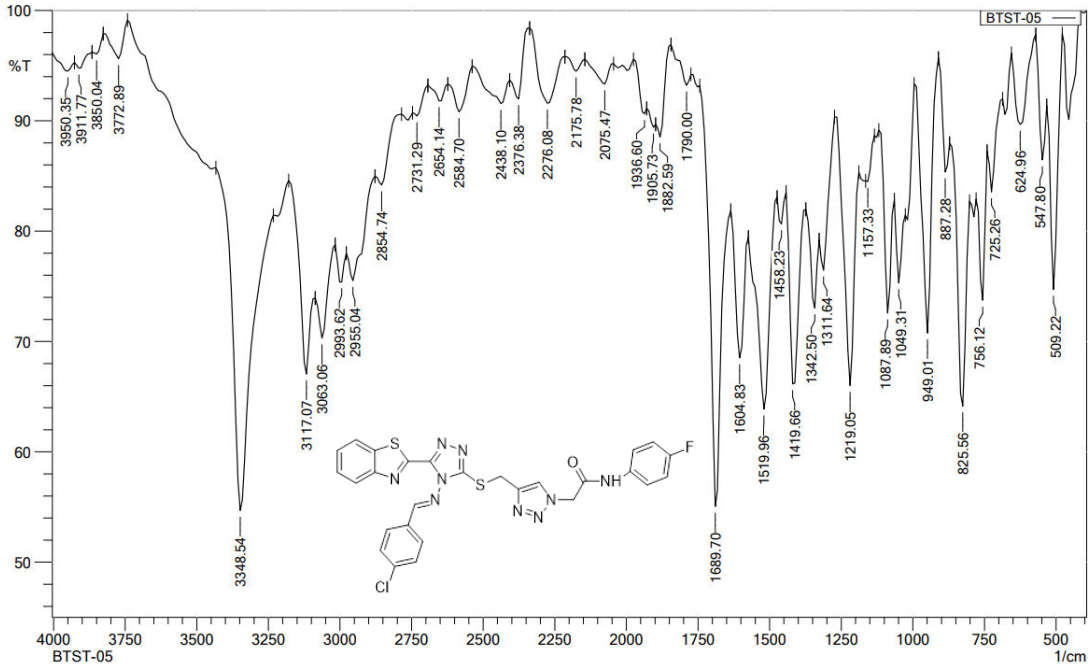

Figure 32: Representative FT-IR spectrum of compound 10e

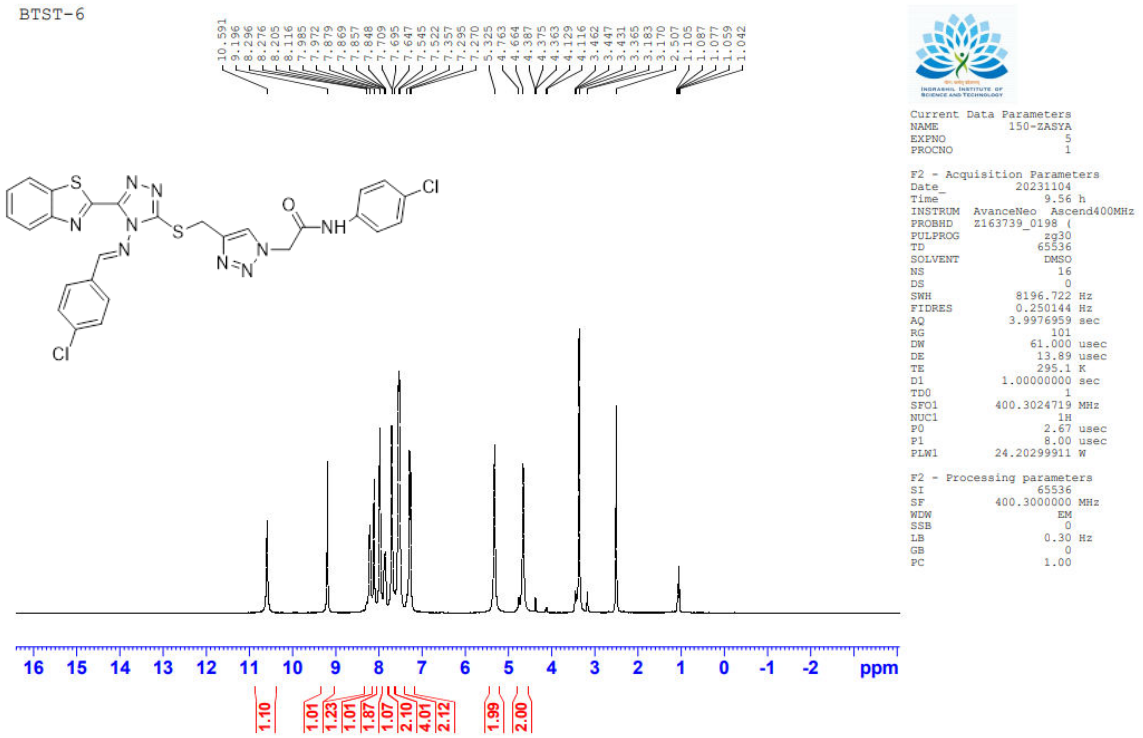

Figure 33: Representative ^{1}H NMR spectrum of compound 10f

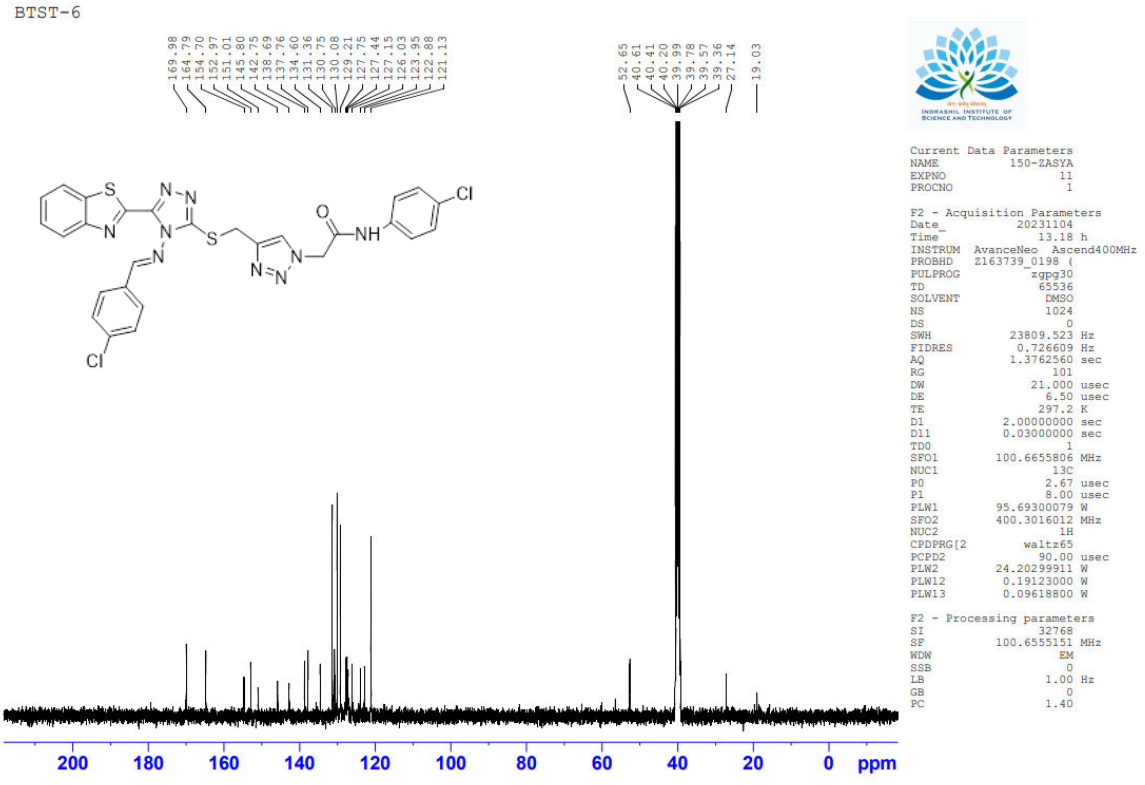

Figure 34: Representative ^{13}C NMR spectrum of compound 10f

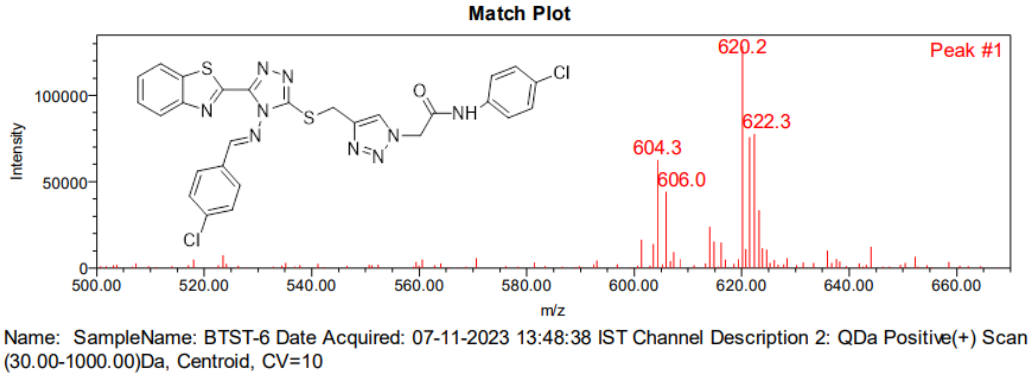

Figure 35: Representative mass spectrum of compound 10f

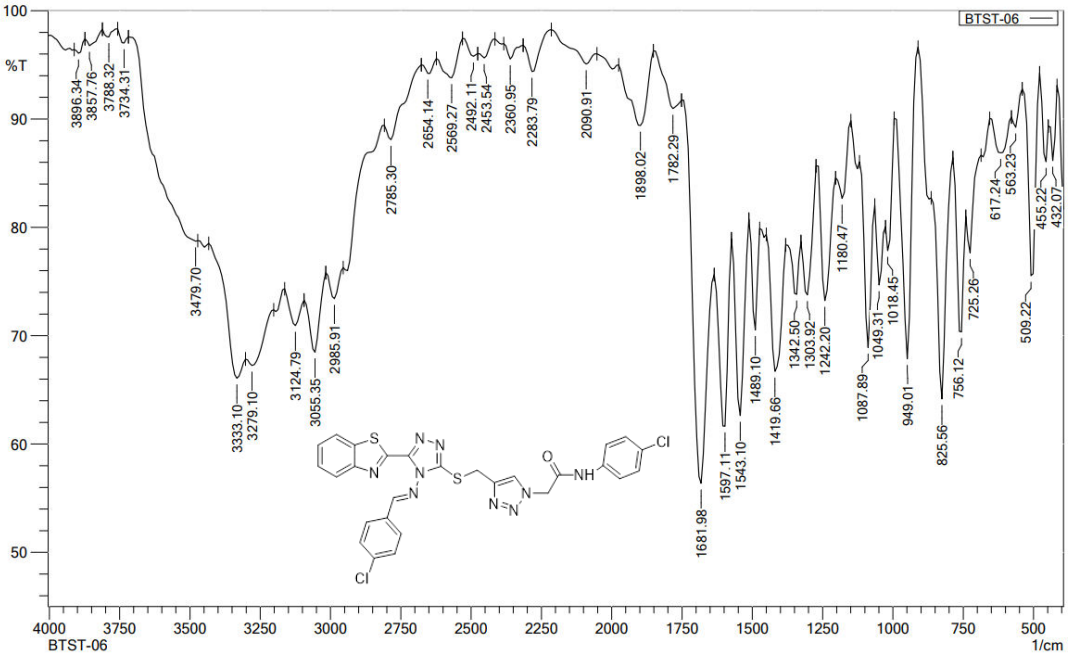

Figure 36: Representative FT-IR spectrum of compound 10f

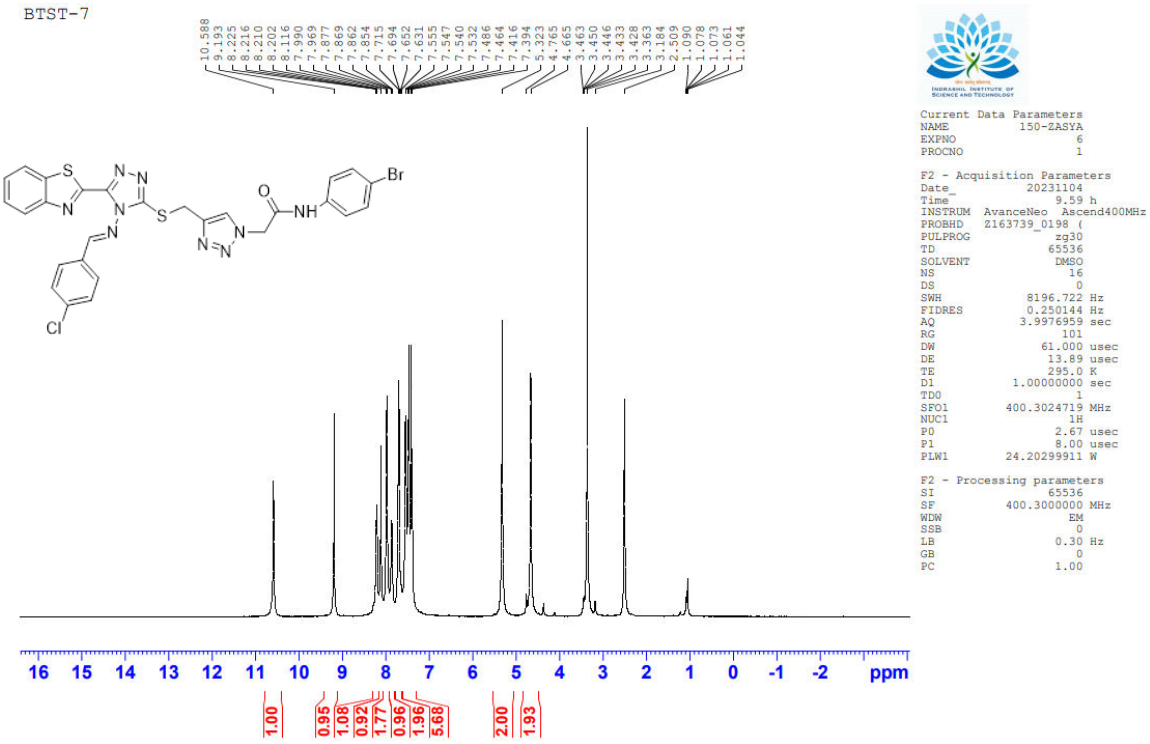

Figure 37: Representative ^{1}H NMR spectrum of compound 10g

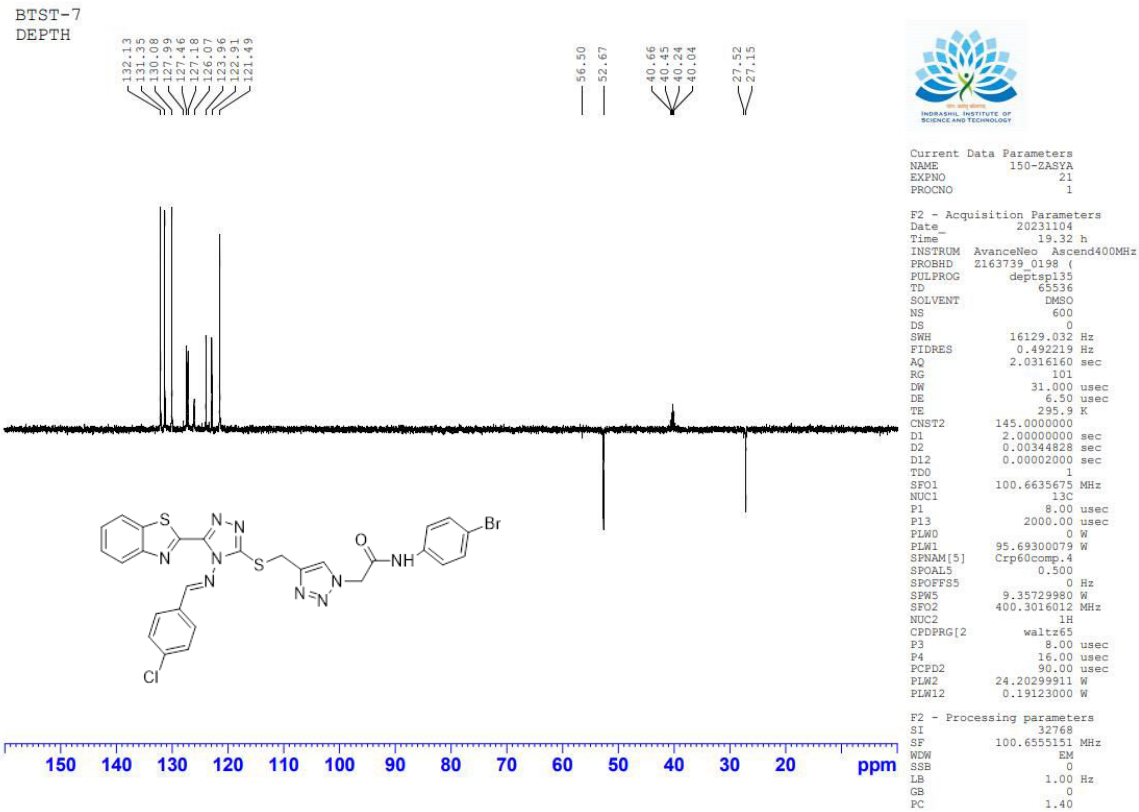

Figure 38: Representative ^{13}C DEPT-135 NMR spectrum of compound 10g

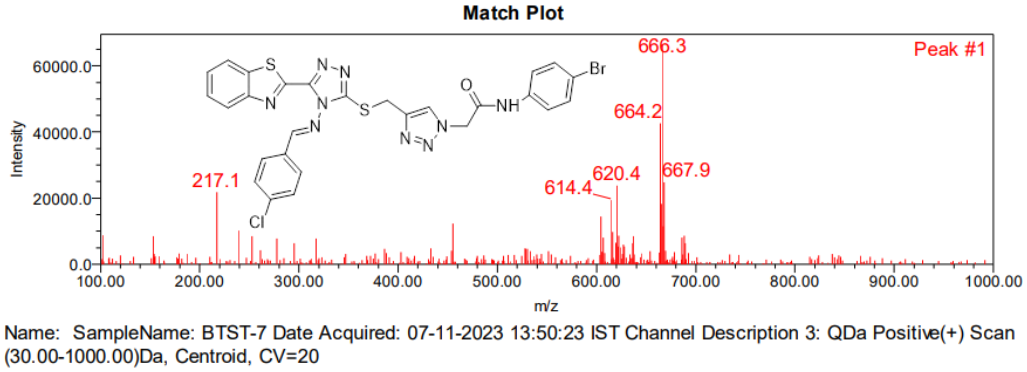

Figure 39: Representative mass spectrum of compound 10g

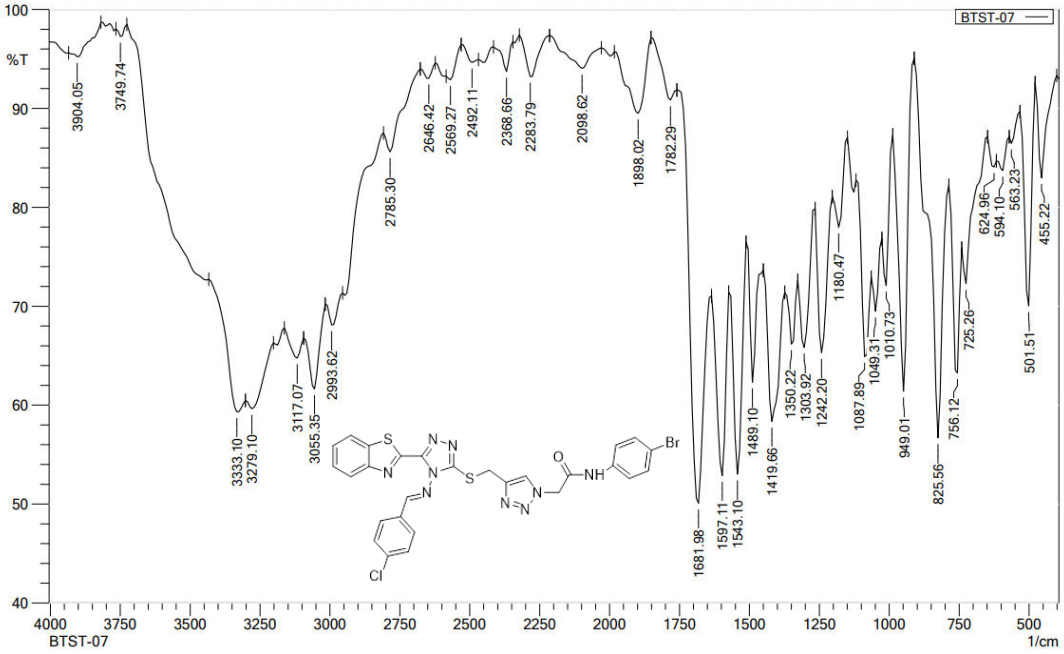

Figure 40: Representative FT-IR spectrum of compound 10g

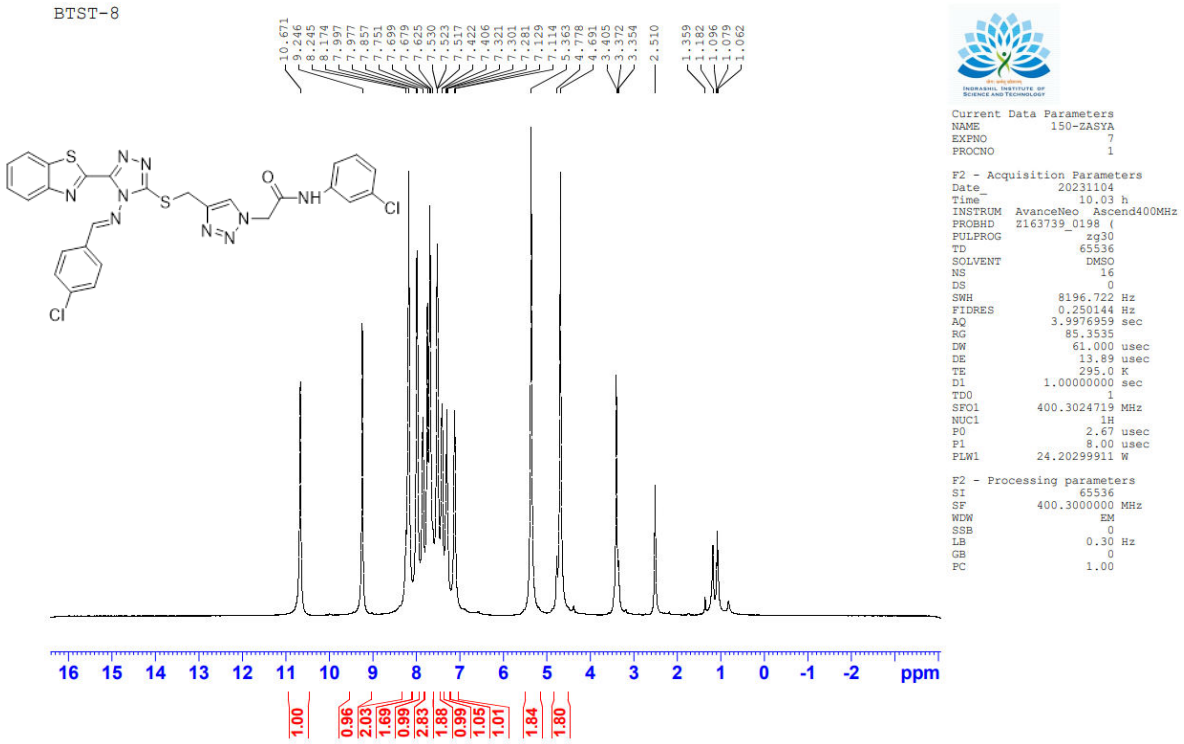

Figure 41: Representative ^{1}H NMR spectrum of compound 10h

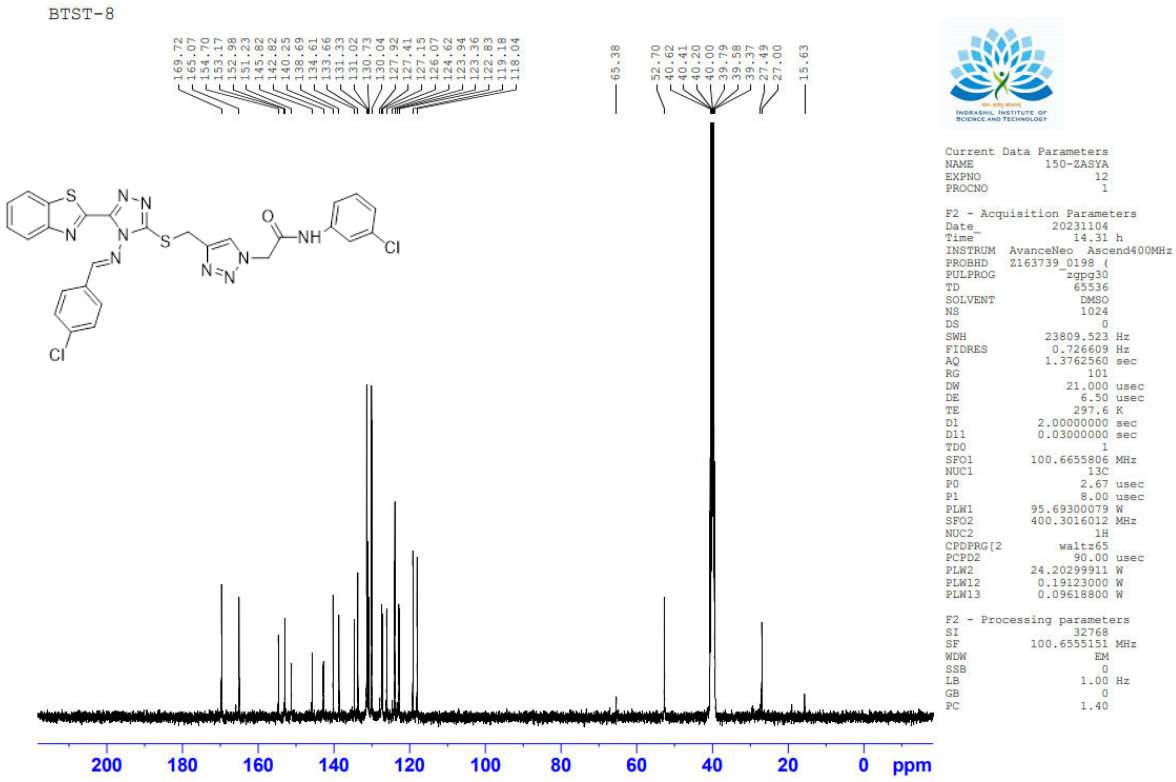

Figure 42: Representative ^{13}C NMR spectrum of compound 10h

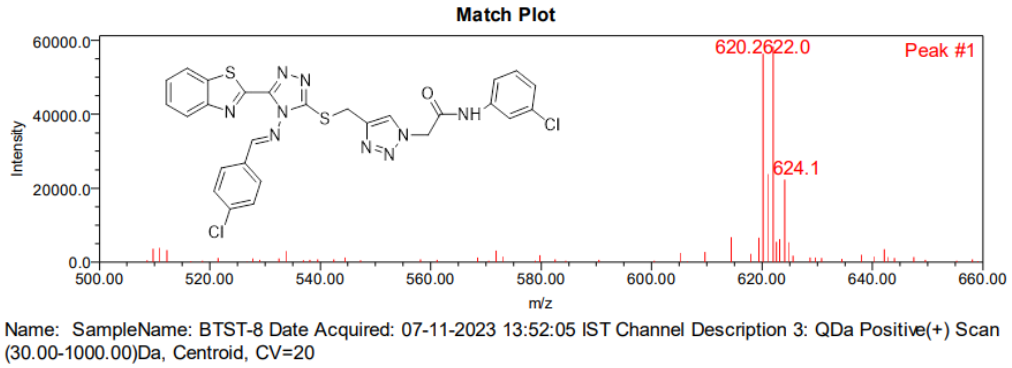

Figure 43: Representative mass spectrum of compound 10h

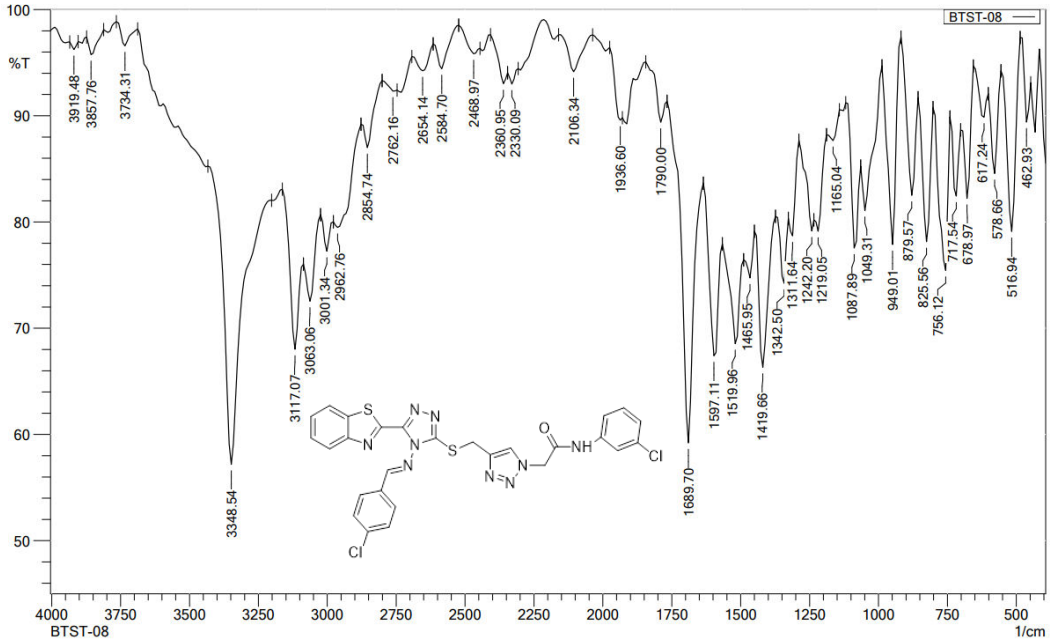

Figure 44: Representative FT-IR spectrum of compound 10h

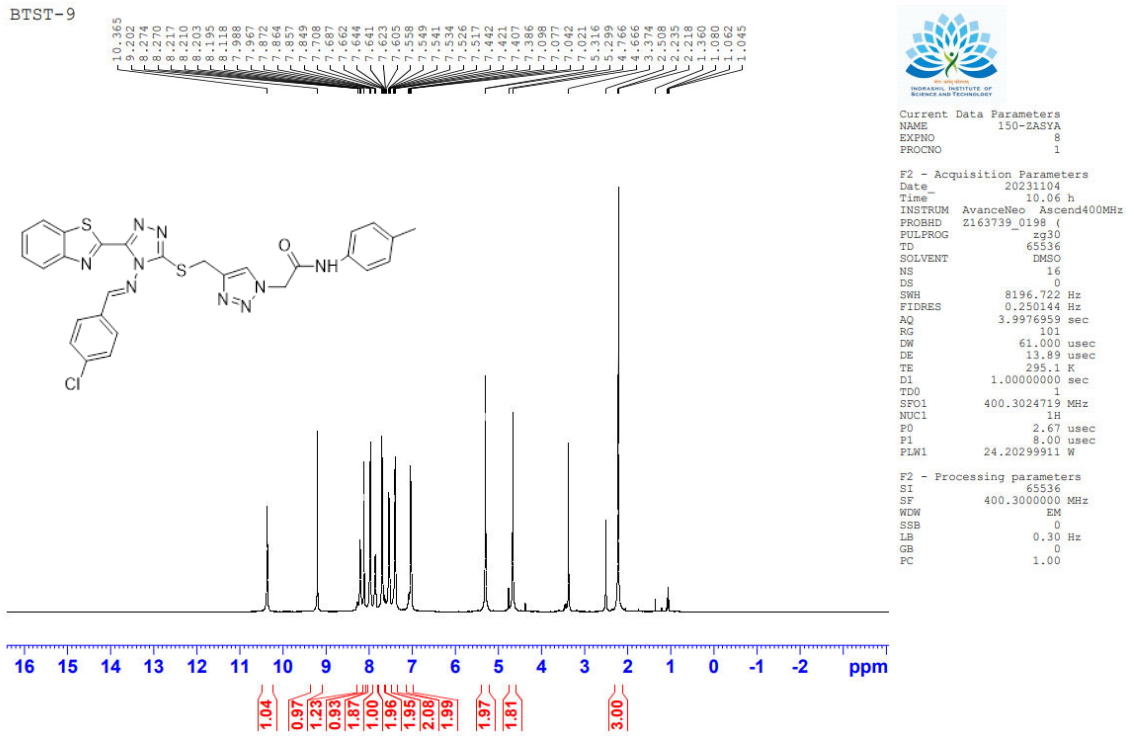

Figure 45: Representative ^{1}H NMR spectrum of compound 10i

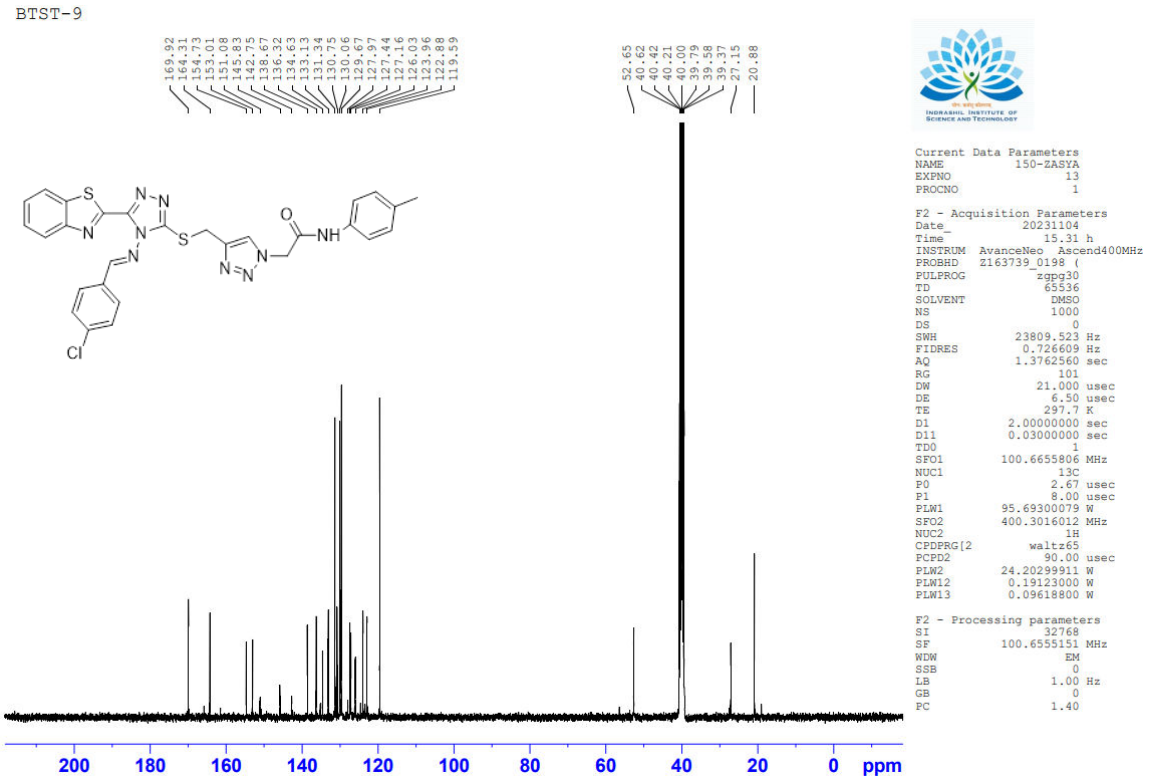

Figure 46: Representative ^{13}C NMR spectrum of compound 10i

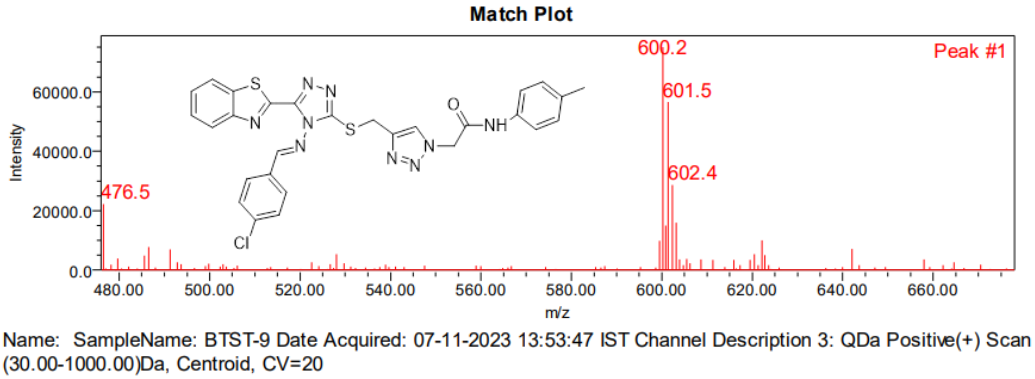

Figure 47: Representative mass spectrum of compound 10i

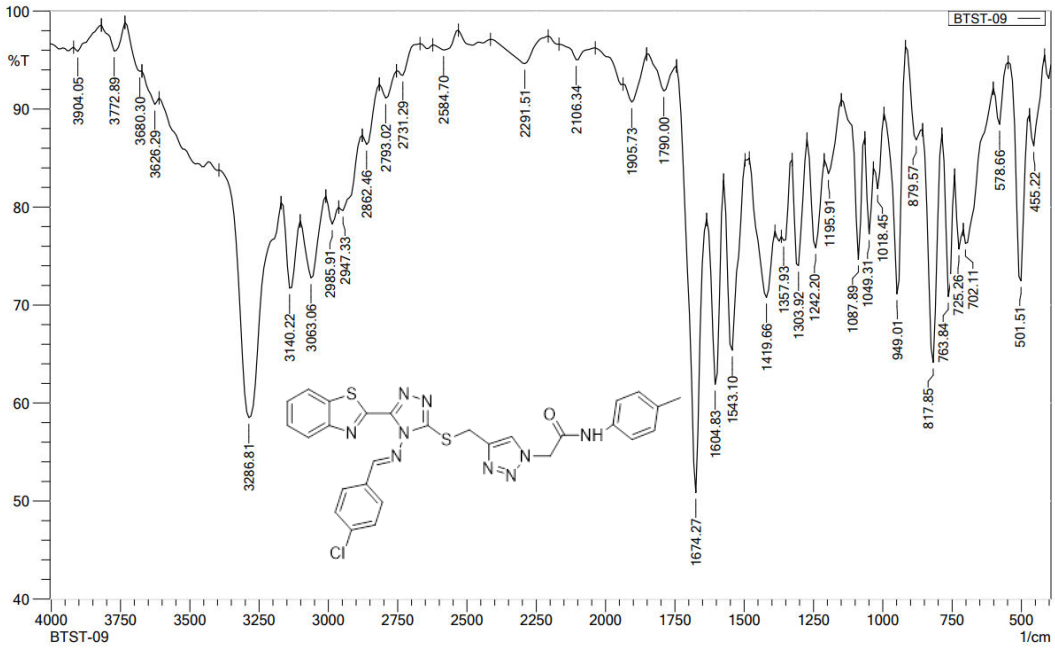

Figure 48: Representative FT-IR spectrum of compound 10i

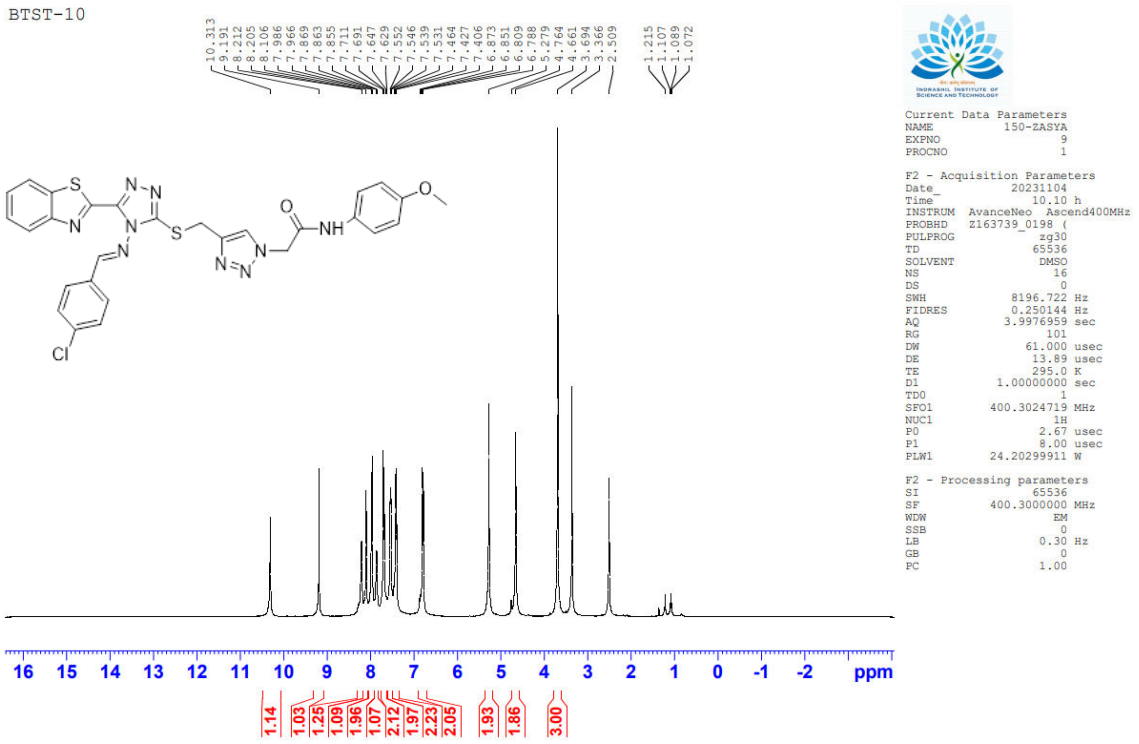

Figure 49: Representative ^{1}H NMR spectrum of compound 10j

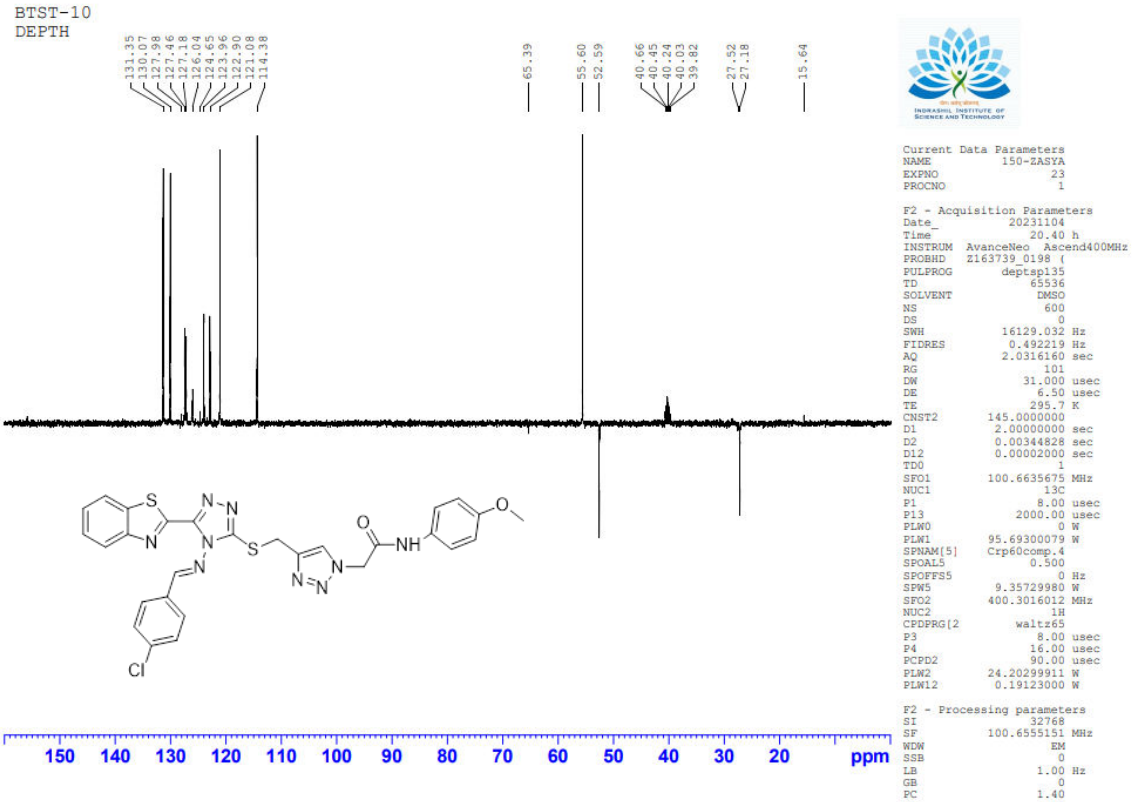

Figure 50: Representative ^{13}C NMR spectrum of compound 10j

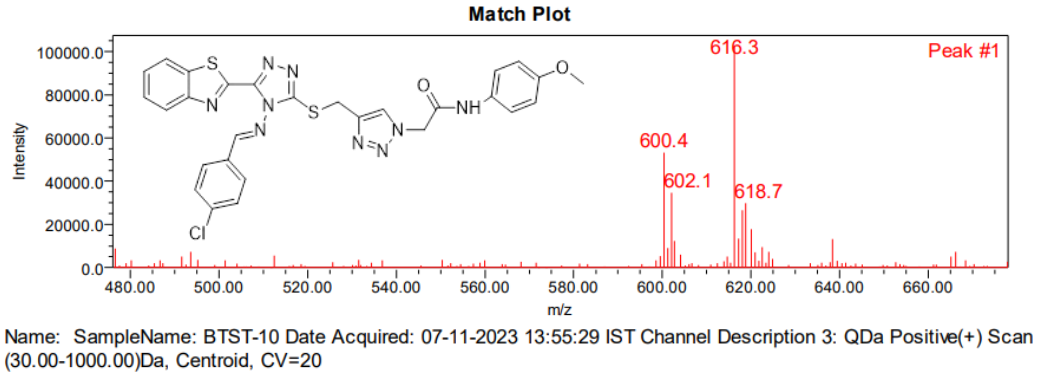

Figure 51: Representative mass spectrum of compound 10j

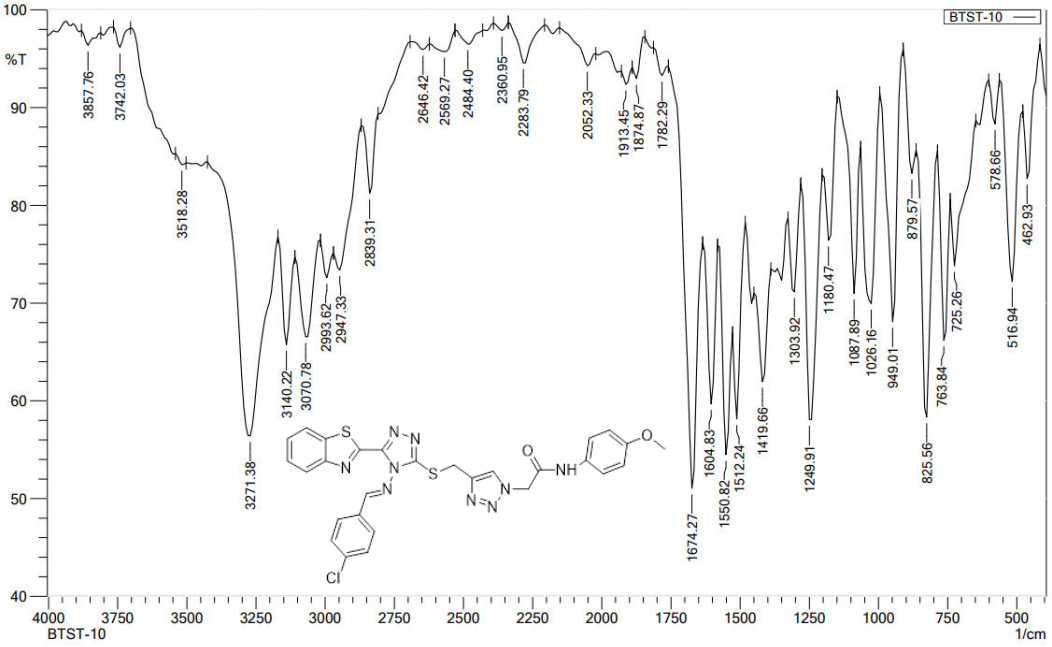

Figure 52: Representative FT-IR spectrum of compound 10j